Ann. Rev. Biochem. 1979. 48:327–86

REGULATION OF OXYGEN AFFINITY OF HEMOGLOBIN:

Influence of Structure of the Globin on the Heme Iron

◆12012

M. F. Perutz

Medical Research Council Laboratory of Molecular Biology, Cambridge, CB2 2QH, England

---

CONTENTS

0066-4154/79/0701-0327$01.00

PERSPECTIVES AND SUMMARY

Vertebrate hemoglobins (Hb's) are in equilibrium between two alternative structures, the deoxy or T and the oxy or R structure, whose oxygen dissociation constants differ by the equivalent of over 3 kcal/mol heme. The dissociation constant of myoglobin (Mb) is slightly higher than that of the R structure. Many years ago David Keilin asked me how nature could use the same heme for so many different functions, simply by attaching it to different proteins. In this review I try to answer a small part of his question: how does the structure of the globin influence the oxygen affinity of the heme?

Ideally, the problem should be approached by accurate X-ray analyses of the heme geometries in these proteins, but even the best resolution available does not allow bond lengths to be determined with the required accuracy (± 0.005 Å). The exact bond lengths must therefore be inferred from X-ray analyses of synthetic porphyrins designed to mimic the states of the heme in Hb. In deoxyHb the iron is five-coordinated and high-spin, while in HbO_2 it is six-coordinated and low-spin. Six-coordinated hemes are usually planar or nearly so, while in five-coordinated ones the iron lies at the apex of a square pyramid whose base is formed by the pyrrollic nitrogens. The influence of coordination number and spin on the height of the pyramid and on the Fe–N bond lengths can be gauged from Table 1.

The table shows that both bond lengths and height of the pyramid increase on going from six- to five-coordination and from lower to higher spin. In synthetic iron chelates differences in iron ligand bond lengths are

Table 1 Influence of the coordination number on the properties of Fe–N bonds

Valency of Fe	Coordination number	Spin (*S*)	$Fe–N_{porph}$ (Å)	Fe–Ct (height of pyramid) (Å)
2	6	0 (low)	1.98–2.00	0–0.2
2	6	2 (high)	2.06	0
2	5	0 (low)	2.00	0.2
2	5	2 (high)	2.07–2.09	0.45 (± 0.06)
3	6	1/2 (low)	1.99	0–0.1
3	6	5/2 (high)	2.04	1–0.3
3	5	5/2 (high)	2.07	0.45 (± 0.06)

accompanied by spin changes, and vice versa, even when the coordination number and nature of the ligands remains unaltered.

As far as limited resolution allows us to judge, these general principles are borne out by the heme geometries of Mb and Hb. In their deoxy forms the iron atoms are displaced from the mean porphyrin plane by 0.55–0.63 Å; some of this displacement is probably due to doming of the porphyrin. In six-coordinated forms the iron atoms lie closer to the porphyrin plane. The hemes lie in isolated pockets into which they are wedged tightly by about 16 side chains of the globin; these allow no movement of the iron atom and the proximal histidine relative to the porphyrin plane without a change in tertiary structure of the globin. In the β-subunits of the T structure the oxygen site is obstructed by the distal valine, and this obstruction, again, cannot be cleared without a change of tertiary structure of the globin. This suggests that the oxygen affinity could be regulated by simple mechanical devices that impede the movement of the iron and of the distal valine relative to the heme center in different ways or by different degrees in the T and R structures. Comparison of the tertiary structures of deoxyHb and HbCO suggest that this is true, combination with oxygen being unhindered in the R, and hindered in the T structure. Conversely the displacement of the iron with its proximal histidine and, in the β-subunits only, of the distal valine from the heme center, appear to be the main factors regulating the allosteric equilibrium between the T and R structures.

Convincing chemical evidence for a restraint which impedes the movement of the iron towards the porphyrin plane on ligand binding came from HbNO, where a forced transition from the R to the T structure tore the heme iron away from its bond with the proximal histidine in the α-subunits. To measure the energy equivalent of the restraint, we turned to metHb derivatives in which there exists a thermal equilibrium between two alternative spin states. A switch in quaternary structure from R to T is shown to bias that equilibrium toward higher spin, i.e. toward longer Fe–N bonds. Conversely, the higher the spin, the lower the energy needed to effect the switch to the T structure. Accurate measurements of thermal spin equilibria of carp azide metHb over a wide temperature range showed that the change in spin equilibrium is equivalent to a free energy change of 1 kcal/mol heme averaged over the tetramer, but it seems more likely that the spin change occurs mainly in one pair of subunits (possibly the α) with a free energy change of 2 kcal/mol heme. This suggests that restraint of the heme iron's movement may be dominant in regulating the oxygen affinity in one pair of subunits and steric hindrance of the ligand site by the distal valine in the other. Azide metMb at room temperature has a higher spin than azide metHb in the R structure, which is consistent with the lower oxygen affinity of myoglobin.

Can steric restraint of the type envisaged here really lower the oxygen affinity? Steric restraint by the globin has been mimicked in synthetic iron porphyrins by attaching a methyl group to the proximal imidazole in position 2, i.e. at the carbon next to the Fe–N_ϵ bond. Close contact between this methyl and the porphyrin nitrogen hinders the approach of the histidine and of its attached iron atom to the porphyrin plane. This hindrance lowers the oxygen affinity by about the same factor as the transition from the R to the T structure in Hb, which shows that the proposed mechanism is chemically viable.

INTRODUCTION

The hemoglobins are essential to the life of all vertebrates; they also occur in some invertebrates and in the root nodules of leguminous plants. They all carry the same prosthetic heme group, iron (II) protoporphyrin IX, associated with a polypeptide chain of between 136 and 153 residues. In all of them the ferrous iron of the heme is linked to N_ϵ of a histidine, the porphyrin is wedged into its pocket by a phenylalanine, and about 35 other specific sites along the polypeptide chain are occupied by nonpolar residues. These requirements seem to suffice to determine the characteristic fold of the polypeptide chain that is common to the hemoglobins of all species (Figure 1). For the rest, the amino acid sequences of the hemoglobins are variable, the number of amino acid differences between any two species rising with their distance of separation on the evolutionary tree (1–3).

The carriage of oxygen by the hemoglobins is based on the ability of their ferrous iron to combine reversibly with molecular oxygen instead of being irreversibly oxidized; the heme and the amino acid to which the iron is linked are the same in all hemoglobins, but their oxygen affinities vary widely. The affinity is expressed as p_{50}, the partial pressure of oxygen, in mm Hg, at which the solution is half saturated with oxygen. The highest affinity (0.004 mm Hg) has been recorded in *Ascaris* hemoglobin and the lowest (~1000 mm Hg) in certain fish hemoglobins at acid pH. This 250,000-fold variation, equivalent to a difference in binding energy of 7 kcal/mol, shows that the structure of the globin has a strong influence on the chemical affinity of the heme iron.

The oxygen affinities of single-chain hemoglobins, such as those found in the body fluids of invertebrates and in the cytoplasm of vertebrate muscle (myoglobin), are generally independent of the ionic composition of the solution, and their oxygen equilibrium curves are rectangular hyperbolae. On the other hand, the hemoglobins found in the erythrocytes of vertebrates are tetrameric, consisting of four hemes plus two pairs of polypeptide chains of unequal length and different amino acid sequence. Their oxygen affinities

rise with increasing oxygen saturation so that their oxygen equilibrium curves are sigmoid. Under physiological conditions the rise in oxygen affinity of human hemoglobin between zero and full oxygen saturation is about 500-fold, corresponding to a free energy difference of 3600 cal/mol heme. This is known as the free energy of heme-heme interaction. Its magnitude and the value of p_{50} vary with pH and with the concentrations of CO_2, Cl^-, HPO_4^{2-}, 2,3-diphosphoglycerate (DPG), and other phosphate esters. A change in the activity of any of these agents affects the affinity of hemoglobin for all the others. The interactions just described are known collectively as the cooperative effects of hemoglobin. They are a property of the hemoglobin tetramer and vanish upon splitting of the molecule into two dimers or into free subunits. This shows that they are somehow related to the bonds between the subunits.

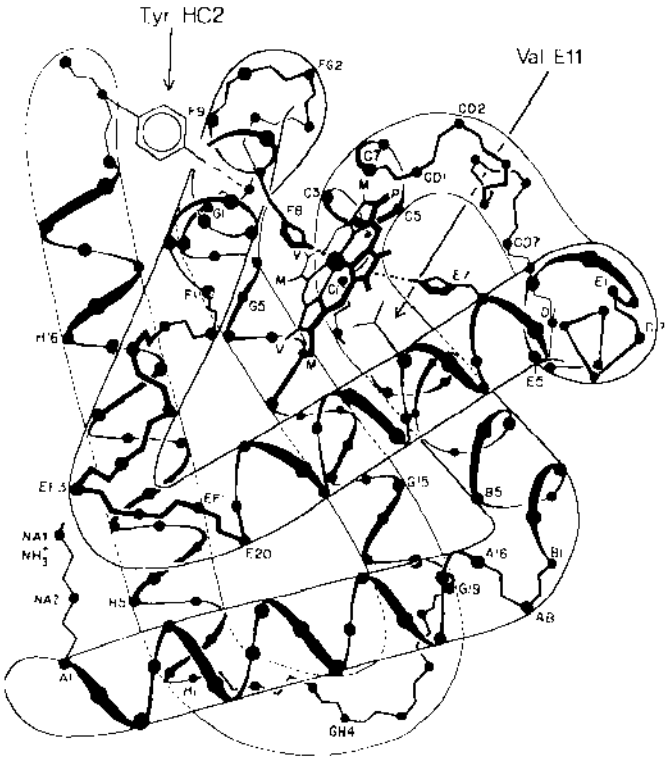

Figure 1 Secondary and tertiary structures characteristic of the hemoglobins. Helical segments are denoted *A* to *H;* nonhelical ones *NA, AB* to *GH,* and *HC.* Residues along segments are numbered in sequence. The diagram shows the proximal His F8, the distal His E7, and the distal Val E11, and Tyr HC2 which play an important part in the allosteric mechanism.

Structure analysis aims at interpreting these remarkable properties in stereochemical terms. We now know that the cooperative effects arise from a transition between two alternative structures, the deoxy or T and the oxy or R structure. These differ in the conformation of the individual subunits, the tertiary structure, and the relative arrangement of the four subunits, the quaternary structure. In the R structure the oxygen affinity is slightly higher than in free α- and β-subunits, but in the T structure it is several hundred times lower. By what kind of mechanism does the change in the structure of the globin influence the chemical reactivity of the heme iron? Or conversely, by what kind of mechanism does the combination of the heme iron with oxygen change the structure of the globin? There must be a stereochemical change at the heme accompanying the reaction with oxygen which sets in train the transition from the R to the T structure. Conversely the low oxygen affinity of the T structure must be due to constraints of the globin which oppose this change. I now review the stereochemical changes at the heme brought about by the reaction of oxygen with model compounds designed to mimic hemoglobin.

STEREOCHEMISTRY OF IRON PORPHYRINS AND RELATED COMPOUNDS

Coordination of the Iron Atom

The ferrous ion contains six and the ferric ion five valency (d) electrons which can populate the orbitals shown in Figure 2. In octahedral or square pyramidal complexes the T_g orbitals are oriented between the bond direction, so that repulsion by the iron ligands is minimized, and their energy remains low. The E_g orbitals point in the bond direction. Repulsion by the ligand atoms causes their energy to rise with the strength of the bonds to the iron atom. In five-coordinated iron porphyrins the energy of the E_g orbitals is usually low enough for them to be populated, so that the ferrous complexes contain four and the ferric ones five unpaired electrons, which make them strongly paramagnetic or "high-spin." In six-coordinated iron porphyrin complexes the distribution of electrons varies with the strength of the bonds to the distal ligands, with strong, short bonds favoring "low-spin", i.e. weakly paramagnetic or diamagnetic states, and weak, long bonds favoring high-spin states. There also exist states of intermediate spin with two unpaired electrons in the ferrous and three in the ferric state; in iron porphyrins these have been observed only in four-coordinated or very weakly five-coordinated complexes where the d_{z^2} orbital is occupied but the $d_{x^2-y^2}$ orbital remains empty.

In all Hb's the iron is coordinated to four nitrogens of the porphyrin and to N_ϵ of the proximal histidine. In deoxyHb the iron is five-coordinated and paramagnetic with a spin of $S = 2$. We now know the structures of

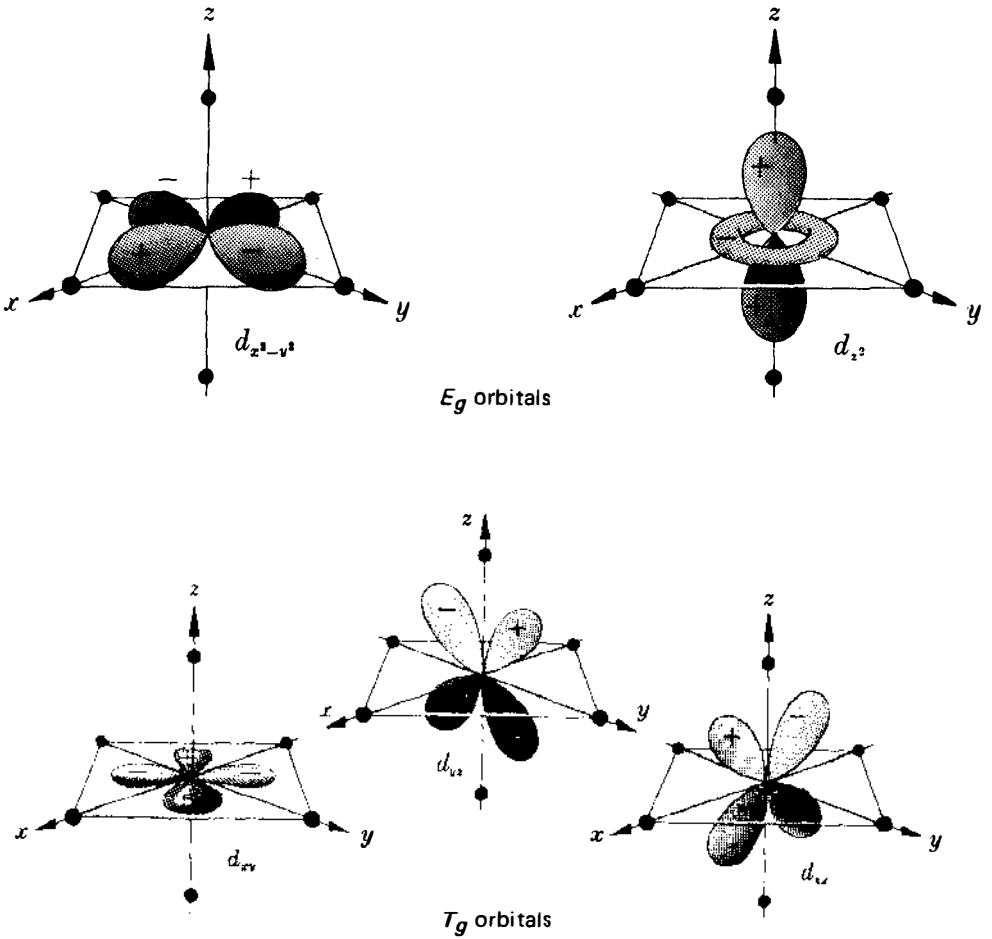

Figure 2 *d* orbitals of iron. Note that the T_g orbitals are directed at 45° to the bonds with the octahedrally coordinated ligands, while the E_g orbitals point in the bond directions. They normally have higher energies than the E_g's.

two model compounds of deoxyHb, both having as the axial base 2-methylimidazole, which is hindered from close approach to the porphyrin by the bulk of its methyl group (Figure 3 and Table 2), (4–6). In (2-methylimidazole)*meso*-tetraphenylporphinato Fe(II), (2-MeImTPPFeII for short) the porphyrin is markedly domed toward the imidazole, so that the plane of the four nitrogen atoms lies 0.13 Å above the plane of the 24 atom porphyrin skeleton. The iron lies (0.418 ± 0.005) Å above the plane of the nitrogens. The average length of the bonds from the iron to the

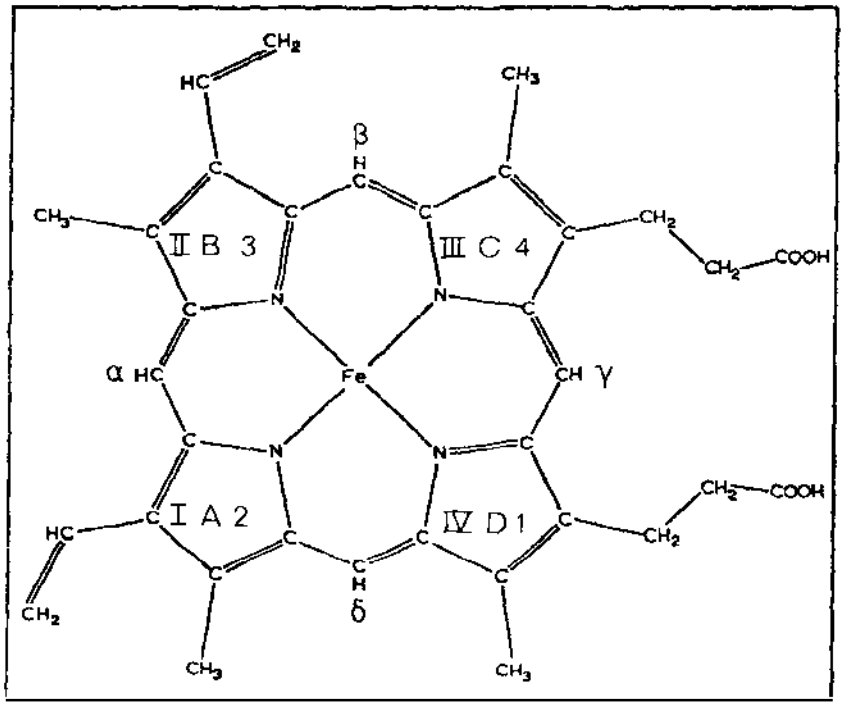

Figure 3a Fe-protoporphyrin IX. The arabic numbers are those adopted in (7, 8), the roman ones are from (9–11), and the letters are from (12).

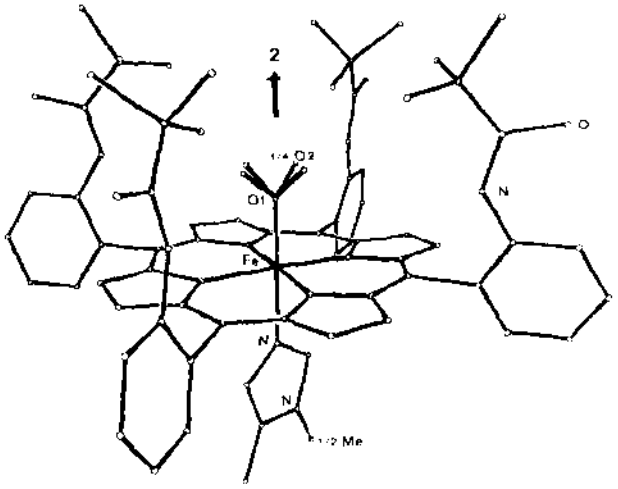

Figure 3b The oxygenated picket fence complex of Collman and his collaborators. The terminal groups of the "pickets" are methyls. This has the sterically unhindered 1-methylimidazole as the proximal ligand. Reproduced, with permission, from (13).

Table 2 Geometry of iron porphyrins

Compound	Coordination number	Spin (S)	Fe–N_{porph}[b] (Å)	Fe–Ct[c] (Å)	Ref.
2-MeIm TPP Fe II	5	2	2.086 (4)	0.42	4, 6
2-MeIm piv PP Fe II	5	2	2.072 (5)	0.40	7
2-MeIm piv PP Fe II O_2	6	0	1.996 (4)	0.09	14
1-MeIm piv PP Fe II O_2	6	0	1.980 (10)	−0.03	15
bis THF TPP Fe II	6	2	2.057 (4)	0	114
1-MeIm TPP Fe II NO	6	1/2	2.008 (12)	−0.07	16
TPP Fe II NO	5	1/2	2.001 (3)	−0.211	17
bis Im TPP Fe III Cl^-CH_3OH	6	1/2	1.989 (4)	0	4, 6
bis H_2O TPP Fe III	6	5/2	2.045 (8)	0	18
TPP Fe III N_3^-	5	5/2	2.067	−0.45	4
Pyr TPP Fe III N_3^-	6	1/2	1.990	−0.03	4

[a] TPP: tetraphenylporphyrin; piv: pivalamido; Me–Im: methylimidazole; THF: tetrahydrofuran.

[b] Numbers in brackets are RMS errors.

[c] Ct: center of porphyrin nitrogens; Fe–Ct: displacement of iron perpendicular to the plane of the four nitrogens, positive toward imidazole, negative toward O_2, NO, N_3^-, or SCN^-.

porphyrin nitrogens is 2.086 (±0.004) Å and the length of its bond to the imidazole nitrogen is 2.161 (±0.005) Å.[1] The second model is (2-methylimidazole)*meso*-tetra(α,α,α,α-*o*-pivalamidophenyl)porphinato-Fe(II), (2-MeImTpivPPFeII for short). Here the porphyrinato skeleton is less domed, so that the plane of the four nitrogens lies only 0.03 Å from the mean plane of the skeleton. The iron lies 0.399 Å above the plane of the four nitrogens. The average length of the bonds from the iron to the nitrogens is 2.072 (±0.005) Å and the length of its bond to the imidazole nitrogen is 2.095 (±0.006) Å. This compound is generally known as the "picket fence" complex because the pivalamidephenyl side chains form a fence around the iron ligand site. The crystal structures of two different oxygen adducts of this complex have now been determined, one having the sterically unhindered 1-methylimidazole as the fifth heme ligand, which might be regarded as a model of HbO_2 in the R structure (8), and the other with the sterically hindered 2-methylimidazole as the fifth ligand, which might be regarded as a model of HbO_2 in the T structure, because repulsion between the methyl group in the 2 position and the porphyrin nitrogens appears to mimic the restraints of the globins. In both structures the bonds from the iron to the porphyrin nitrogens are shorter by 0.09 Å (with an error of ±0.006 Å for the 2-MeIm compound) than in the oxygen-free complexes. In the unhindered complex the porphyrinato skeleton is slightly ruffled, so that neighboring methine carbons are displaced by 0.13 Å above

[1] See Fig. 8b, p. 354.

and below the mean porphyrinato plane, and the iron atom is displaced by 0.03 Å from the plane of the four nitrogens toward the oxygen ligand. In the sterically hindered complex the porphyrinato skeleton is buckled with a mean displacement from the least squares plane of 0.066 Å and the iron atom is displaced by 0.086 Å toward the imidazole ligand. In the unhindered complex the sum of Fe–N_{Im} and Fe–O separations is 3.813 Å; in the hindered one the sum is 4.005 Å, the Fe–Im distance being 0.10 and the Fe–O distance 0.15 Å longer, consistent with its lower oxygen affinity (see section on implications for heme-heme interaction).

In summary, analysis of these structures has shown that the iron porphyrin bonds in models designed to mimic deoxyHb are longer by 0.09 Å than in those designed to mimic HbO_2. In the latter the iron and porphyrin atoms lie within 0.1 Å of one plane, while in the former the iron lies at the apex of a pyramid with the four porphyrin nitrogens as its base. The exact height of the pyramid and the doming of the four nitrogens relative to the rest of the porphyrin depend on the angle that the plane of the imidazole makes with the N–Fe–N bonds and also on crystal packing. Similar effects are seen in ferric porphyrins. Six-coordinated low-spin complexes are planar, with Fe–N_{porph} distances of 1.99 Å; five-coordinated high spin ones are pyramidal, with Fe–N_{porph} distances of 2.067 Å and displacements of the iron from the mean porphyrin plane of about 0.45 Å. These differences in geometry arise from two effects: van der Waals repulsion of the axial ligands by the porphyrin nitrogens, and repulsion between the E_g orbitals of the iron and the π orbitals of the porphyrin. The steric effect of a change in the number of axial ligands without change of spin is exemplified by the structures of two ferrous nitrosyl porphyrins: (1-methylimidazole)-$\alpha,\beta,\gamma,\delta$-tetraphenylporphinato Fe(II)NO (1-MeImTPPFeIINO) and the same complex without 1-methyl methylimidazole (TPPFeIINO). Both complexes have spins of $S = 1/2$. In the six-coordinated one the iron is displaced from the the porphyrin plane toward the NO by 0.07 Å, but in the five-coordinated one that displacement is increased to 0.21, even though the mean Fe–N_{porph} bond lengths have increased by less than 0.01 Å. The iron is displaced further from the porphyrin plane because repulsion between the porphyrin nitrogens and the NO is no longer balanced by repulsion between the porphyrin nitrogens and the imidazole nitrogen. Note, however, that the iron in this five-coordinated *low-spin* complex is displaced by only 0.21 Å, while in the five-coordinated *high-spin* TPPFeIII N_3^- the displacement of the iron is 0.45 Å. It has been argued that repulsion between the fifth ligand and the porphyrin nitrogens is more important than spin in determining the displacement of the iron from the porphyrin plane. If that were true, then the displacement of the iron in TPPFeII NO should be greater than in TPPFeIII N_3^-, because it has the shorter Fe–N (ligand) distance (1.743 as against 1.91 Å), so that steric repulsion is greater in the

nitrosyl complex. However, its Fe–N_{porph} distances are 2.001 Å, as against 2.065 Å in the azide complex, so that the iron is displaced more than twice as far in the latter.

The steric effects of filling the d_{z^2} and $d_{x^2-y^2}$ orbitals in turn can be gauged from several other comparisons. In TPP bisImFeIII both orbitals are empty, Fe–N_{porph} = 1.997 Å and Fe–N_{Im} = 2.014 Å. In 1-MeImTPPCoII the $d_{x^2-y^2}$ orbitals are empty and the d_{z^2} orbitals are filled; Fe–N_{porph} = 1.997 Å, the same as before, but Fe–N_{Im} = 2.157 Å, an increase of 0.143 Å.

It is also interesting to compare the position of the metal atom relative to the porphyrin ring in 2-MeImTPPFeII where the $d_{x^2-y^2}$ orbitals are filled, with that in 1-MeImTPPCoII where they are empty. In the former the iron lies 0.418 Å out of the porphyrin plane; in the latter only 0.13 Å, which again shows that five-coordination alone does not cause a substantial displacement of the metal if the $d_{x^2-y^2}$ is empty, but that repulsion between the $d_{x^2-y^2}$ orbitals of the metal and the π orbitals of the porphyrin pushes the five-coordinated metal out of the porphyrin plane. [For references to these structures see (6).]

The steric effect of filling the $d_{x^2-y^2}$ orbitals without change in the number of axial ligands is exemplified by the difference between the structures of $\alpha,\beta,\gamma,\delta$-tetraphenylporphinato-bis-imidazoleFeIII and $\alpha,\beta,\gamma,\delta$-tetraphenylporphinato-bis-H_2OFeIII (TPPbisImFeIII and TPPbisH_2OFeIII). Both have planar hemes. The former is low-spin ($S = 1/2$) and has average Fe–N distances of 1.989 Å; the latter is high-spin ($S = 5/2$) and has average Fe–N distances of 2.045 Å. The longer Fe–N distances are due to repulsion between the occupied $d_{x^2-y^2}$ orbitals of the iron and the π orbitals of the porphyrin nitrogens. The balancing effect of the two axial water molecules holds the iron in the porphyrin plane, but the strain which this planarity entails makes the Fe–N distances 0.026 Å shorter than in five-coordinated ferric high-spin complexes. The same planar geometry is found in the ferrous high-spin six-coordinated bis-tetrahydrofuran tetraphenylporphin Fe(II) (bis THF.TPPFeII for short). Again, the Fe–N_{porph} distances of 2.057 (4) Å are shorter by 0.02–0.03 Å than in five-coordinated ferrous high-spin compounds; on the other hand they are distinctly longer than in the ferric TPPbis H_2OFeIII, which shows that the valency of the iron does have a measurable effect on the Fe–N_{porph} distances in high-spin iron porphyrins, though it seems to be without effect in low-spin ones. These six-coordinated high-spin structures have an important bearing on heme proteins, because they show that the porphyrin is flexible, so that the position of the iron relative to the porphyrin plane and the lengths of the Fe–N bonds may be influenced by the constraints that the protein exercises on the distal ligands, and they may therefore differ from those observed in unconstrained model compounds.

Interaction between Structure and Spin State in Iron Chelates

Much can be learned about the influence of steric constraints on the state of the iron from X-ray and magnetic studies of iron chelates in which the iron is coordinated to sulphur, nitrogen, or oxygen. Especially well studied are the iron dithiocarbamates. In all these complexes the iron is coordinated to six potentially strong ligands, so that one would expect them all to be low-spin. However, steric effects which weaken and lengthen the iron ligand bonds may also change the spin state of the iron, so that some of these complexes are intermediate spin ($S = 3/2$), some are high-spin ($S = 5/2$), and others again are balanced in temperature-dependent equilibria between two alternative spin states. In such compounds changes of temperature may bring about changes in iron ligand bond length many times larger than those expected from thermal expansion or contraction alone (Table 3).

In Fe III $(mcd)_3$ the iron is coordinated to six sulphur atoms. (For the formula of this and other complexes quoted here see Table 3.) If this complex is crystallized from water or other hydrogen-bonding solvents, its ground state is $S = 3/2$ with $\langle Fe–S \rangle = 2.443$ Å. If the identical complex is crystallized from benzene its ground state is $S = ½$ with $\langle Fe–S \rangle = 2.318$ Å. The difference is due to the occlusion of solvent molecules in the crystal lattice; hydrogen-bonding solvent molecules may withdraw electrons from the sulphur atoms, thus weakening the Fe–S bonds and favoring higher spin. The complex [Fe II $(6\text{-Me-Pyr})_3$tren$]^{2+}$ in solution is high-spin, while the complex [Fe II $(pyr)_3$tren$]^{2+}$ in solution is low-spin; solutions of complexes in which either one or two of the three pyridines carry methyl groups in position 6 show thermal spin equilibria. The iron atoms are octahedrally coordinated to the three pyridine and the three imino nitrogens. On transition from the high- to the low-spin form, the $Fe–N_{pyr}$ bond lengths shorten by 0.31 Å, and the $Fe–N_{im}$ bond length shortens by 0.20 Å. Note that in the high-spin form these bonds are unusually long; this is believed to be due to overcrowding of the complex by the 6-methyl groups which prevent as close an approach of the iron atoms to the nitrogens as would be needed in a low-spin complex. A similar phenomenon had been found in [tris(2-methyl-1,10-phenanthrolin)Fe II].

In the pair of complexes [Fe III$(acac)_2$trien] PF_6 and [Fe III$(sal)_2$trien]-Cl_2H_2O the iron atoms are coordinated octahedrally to four atoms of nitrogen and two of oxygen, yet the former is pure high-spin and the latter pure low-spin. This difference is brought about, apparently, through the solvent water molecules in the latter which act as proton acceptors in hydrogen bonds from NH groups coordinated to the iron ($H_2O\cdots HN\cdot Fe$). These hydrogen bonds weaken the N–H bonds and thereby strengthen the N–Fe

bonds, so that the complex becomes low-spin, with a reduction of 0.12 Å in the average iron-ligand bond distance. Steric effects of the water molecules may also play a part.

Especially striking are the crystallographic results on the dithiocarbamates, some of which show temperature-dependent spin equilibria, while the spin states of others are independent of temperature. For instance, in

Table 3 Effect of spin on bond distances in iron chelates

Compound	Spin(S)	⟨Fe–S⟩ (Å)		Ref.
Fe III $(mcd)_3 \cdot H_2O$[a]	5/2	2.443		19
Fe III $(mcd)_3 \cdot C_6H_6$[a]	1/2	2.318		19
Fe III Tris (N,N-diethyldithiocarbamate)[b]				
297°K; μ_e = 5.6 BM	high	2.357		20
79°K; μ_e = 2.8 BM	low	2.306		
		Fe–N (pyridine)	Fe–N (imine)	
Fe II $(6\text{-Me-Pyr})_3$ tren $^{2+}$ $(PF_6^-)_2$[c]	5/2	2.282	2.143	21
Fe II $(Pyr)_3$ tren $^{2+}$ $(PF_6^-)_2$[d]	1/2	1.966	1.942	21
		⟨Fe–N⟩	⟨Fe–O⟩	
Fe III $(acac)_2$ trien PF_6^-[e]	5/2	2.136	1.928	22
Fe III $(sal)_2$ trien $Cl^- \cdot H_2O$[e]	1/2	1.968	1.884	22

[a] mcd: morpholinocarbodithioato-SS′

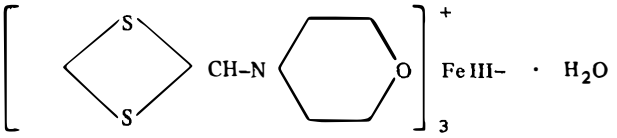

[b] Fe III $(S_2C.N\ Ethyl_2)_3$

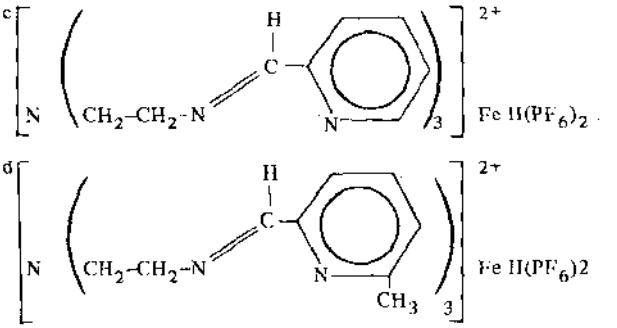

[e] Six-coordinated complexes of Fe III derived from triethylenetetramine (trien) and acetylacetone (acac) or salicyladehyde (sal). In both compounds the iron is coordinated octahedrally to four nitrogens and two oxygens.

$Fe[S_2CN(CH_3)_2]_3$ and $Fe[S_2CN(C_4H_4OH)_2]_3$ the effective magnetic moment μ_{eff} decreases from 4.2 to 2.2 EM on going from 295° to 150°K. This reduction in paramagnetic susceptibility is accompanied by a contraction of the Fe–S bond length by 0.058 Å and 0.062 Å respectively. On the other hand, in

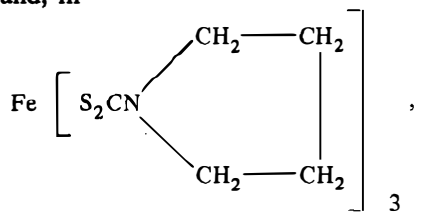

where μ_{eff} remains constant over the same temperature range, the contraction in Fe–S bond length amounts to only 0.008 Å (23). In summary, Table 2 shows that a change of spin is always accompanied by a change in the iron ligand bond lengths and that in the fully low-spin compounds these bonds are shorter by at least 0.1 Å than in the fully high-spin compounds.

The Iron-Oxygen Bond

The nature of the iron-oxygen bond has been the subject of much discussion. The oxygen molecule has 12 valency electrons, and in the ground state these populate seven of the eight molecular orbitals shown in Figure 4. Five pairs go into the five lower lying orbitals, and one electron each goes into the two $1\pi_g^*$ antibonding orbitals. These give the oxygen molecule its spin of $S = 1$.

Pauling & Coryell found HbO_2 to be diamagnetic, whence they argued that the iron oxygen bond should have the resonating structure

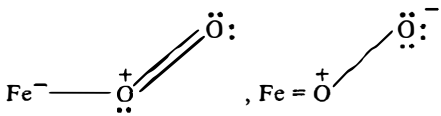

which makes all electrons paired (25). In modern terms this means that the two $1\pi_g^*$ orbitals no longer have the same energy, so that their electrons pair in the single π_y^* which has a lower energy than π_x^*, because it lies at right angles to the Fe–O–O plane. On Pauling's model, the bond between the iron and oxygen would be made by hybridization between the π orbitals of the oxygen and the d_{xz} and d_{yz} orbitals of the iron, with some net transfer of charge from the oxygen to the iron. This model was challenged by J. J. Weiss who suggested that the bond might be ionic between a ferric ion and a superoxide ion, net charge being transferred from the iron to the oxygen ($Fe^{3+}O_2^-$) (26). Experimental support for Weiss' model was first advanced

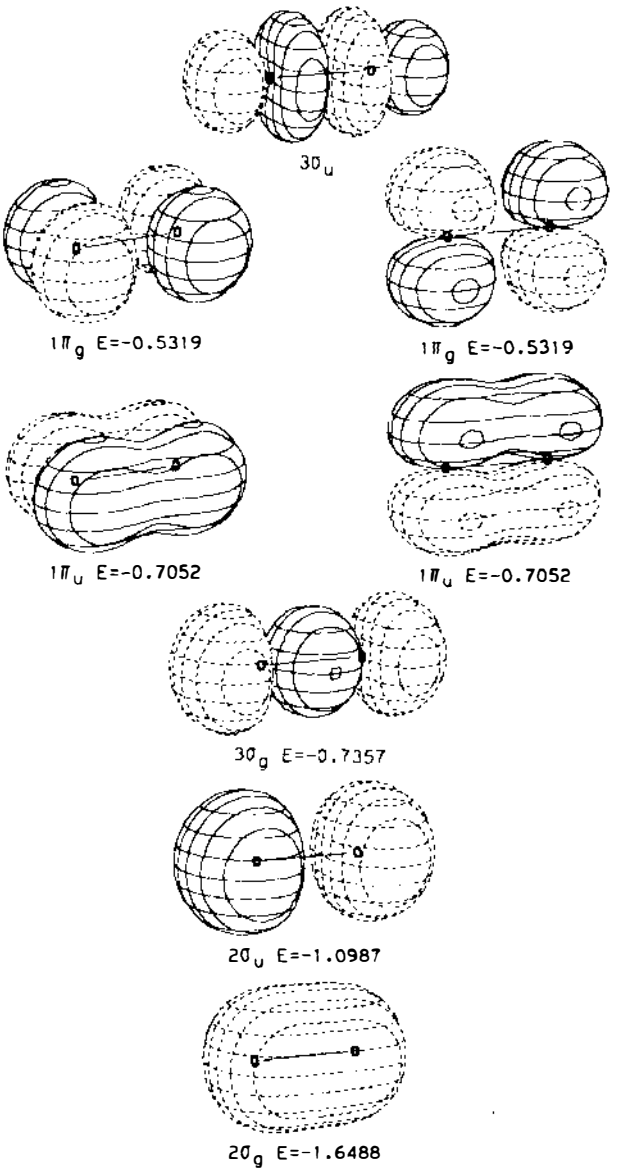

Figure 4 Molecular orbitals of oxygen arranged in the order of their energy. Of the six pairs of p electrons, five pairs fill the five lowest lying orbitals. The remaining pair is split between the two $1\pi g$ orbitals. These are antibonding and are referred to in the text as π_x^* and π_y^*. Reproduced, with permission, from (24).

by Misra & Fridovich (27). They showed the autoxidation of HbO_2 to be a first order reaction depending only on $[HbO_2]$; when epinephrin was added to the solution it was oxidized to adrenochrome, but this oxidation was inhibited in the simultaneous presence of superoxide dismutase and catalase, which suggests that superoxide ion is liberated on autoxidation of HbO_2. Recently, Demma & Salhany (28) have shown that liberation of oxygen by flash photolysis of HbO_2 reduces oxidized cytochrome *c*, and this too is inhibited by superoxide dismutase and catalase. The ($Fe^{3+}O_2^-$) structure is also supported by spectroscopic evidence. The infrared O–O stretching frequency in HbO_2 is 1107 cm^{-1} (29), which is in the superoxide ion range (1150–1100 cm^{-1}), much lower than that of the oxygen molecule (1556 cm^{-1}), and higher than that of a single O–O bond (~800 cm^{-1}). X-ray fluorescence also points to the presence of unpaired electron density on the iron atom (115). Cobalt porphyrins and Hb's combine reversibly with molecular oxygen and provide a probe for exploring the bond in the form of an unpaired electron on the cobaltous d^7 ion. This gives an ESR signal with nuclear hyperfine splitting from which the unpaired electron density can be located. In the deoxy derivatives hyperfine splitting from the Co is combined with that of a single nitrogen atom of the proximal histidine, which shows that the unpaired electron occupies the d^{z^2} orbital pointing toward the histidine. In the oxy derivatives, the nitrogen splitting disappears and the separation of the hyperfine lines due to Co is reduced to about a third. Since that separation is directly proportional to the unpaired electron density on the Co, it is inferred that a substantial fraction of the density has gone to the oxygen (30–32). This has been confirmed by a similar experiment in reverse, using $CoHb^{17}O_2$. ^{17}O has a nuclear spin of $I = 5/2$, so that it should give rise to hyperfine splitting if the unpaired electron density is transferred from the Co to O_2. This is indeed observed, and its magnitude suggests that about 60% of the unpaired electron density is transferred (33). It might be argued that the metal-oxygen bonds might be different in the Fe and Co derivatives, but the similarity of the O–O stretching frequencies, 1107 cm^{-1} for Fe and 1106 cm^{-1} for Co, suggests that they are similar (34). Sadly Weiss died before his prediction was confirmed experimentally. The $Fe^{3+}O_2^-$ model can be reconciled with diamagnetism or weak paramagnetism of the complex by postulating that the transferred *d* electron of the iron pairs with one of the two π^* electrons of the oxygen, and that the spin of the other π^* electron is paired with the odd *d* electron left behind on the iron by antiferromagnetic coupling. The diamagnetism of HbO_2 has recently been challenged by Cerdonio et al, who produced evidence of a low lying triplet state which makes it weakly paramagnetic at room temperature (35, 36). Their observations, though apparently flawless, do raise problems. For example, if oxyhemoglobin at room tempera-

ture had a molar susceptibility per heme of $+2460 \times 10^{-6}$ cgs/mol, as they report, one would expect its NMR spectrum to exhibit hyperfine shifted heme proton resonances, but these have not been observed.

The oxygen adducts of the picket fence complex are definitely diamagnetic (5). The oxygen molecules are bent to the heme axis and lie in four alternative orientations. Due to that disorder it has not been possible to determine the coordinates of the terminal oxygen as accurately as those of the other atoms. In the 1-MeIm complex O–O = 1.16 Å and Fe–O–O = 131°, and in the 2-MeIm complex O–O = 1.22 ± (0.02) Å and Fe–O–O = 129(±1)°. The authors state that they may have underestimated the O–O distance in the unhindered complex by as much as 0.15 Å. The geometry agrees with Pauling's prediction of a bent FeO_2 bond, and the O–O distance is close to that of 1.27 Å, predicted by him in a recent paper. It is slightly shorter than that of 1.34 Å in the superoxide anion, in agreement with the ESR results which show that no more than 2/3 of the density of one electron is transferred from the metal to the antibonding π^* orbitals of the oxygen.

STEREOCHEMISTRY OF HEMOGLOBINS

Monomeric and Dimeric Hemoglobins

COMMON TERTIARY STRUCTURE These hemoglobins include mammalian myoglobin, and hemoglobins of the lamprey, of many invertebrates, and of the root nodules of leguminous plants.

The folding of the polypeptide chain (tertiary structure) of all these hemoglobins is similar to that of sperm whale myoglobin, the first protein structure to be solved (37). It is made up of eight helical and seven nonhelical segments forming a kind of basket for the hemes. Following Kendrew's notation, the helices are lettered A to H and the nonhelical segments NA, AB . . . GH, HC, from the amino to the carboxyl end. Residues along any of the segments are numbered from the amino end. In this way structurally equivalent residues carry the same notation in all hemoglobins regardless of additions or deletions.

Takano (38, 39) has recently refined the structures of sperm whale aquomet- and deoxymyoglobin by X-ray analysis at 2.0 Å resolution, using alternate cycles of real space and Fourier refinement; and Norvell et al (40) have refined the structure of carboxymyoglobin using real space refinement on neutron diffraction data to 1.8 Å resolution. Phillips has solved and refined the structure of oxymyoglobin at 2.0 Å resolution (41), which he is extending to 1.5 Å. The structures of several derivatives of chironomus erythrocruorin have been refined at 1.4 Å resolution (42, 43). The results obtained from these two proteins are quite different.

SURROUNDINGS AND STRUCTURE OF THE HEME IN MYOGLOBIN

The heme is bound to the globin by the mainly covalent bond between the iron atom and Nϵ of the proximal His F8; by hydrogen bonds from one of the propionate side chains to His FG2 and Gln H5, and from the other propionate to Arg CD3; and by about 80 mainly nonpolar interactions with 27 atoms of the globin which lie within less than 4 Å of the heme [see Table II of (44)].

There are three clusters of hydrophobic residues near the heme: one on the side of His E7, another on the side of His F8, and the third at the bottom of the heme. The first cluster accommodates the heme-linked oxygen, but contains enough room beneath His E7 for heme ligands as large as *n*-butyl isocyanide. Takano (38) suggests that the spare room may be needed to let the oxygen molecule in and out. The surface of the heme pocket does not have a hole large enough for oxygen to slip through, and the imidazole of His E7 is like a door that blocks the entrance by leaning against the heme; perhaps it opens by swinging into the free space below.

A xenon atom with a van der Waals radius of 2.2 Å can bind to the second cluster without disturbance to its hydrophobic side chains. The function of the "xenon hole" is unknown and so is that of the third cluster, which is the largest of the three. Takano suggests that they may make the molecule more flexible so that less activation energy is needed for the changes in tertiary structure that may occur on binding and dissociation of oxygen. In met- and deoxy-Mb three of the heme pyrroles seem to be tilted so as to bring their nitrogens closer to His F8, while the fourth seems tilted the other way. This buckling of the pyrroles is not yet very well resolved and needs checking at higher resolution which should be attainable because the X-ray diffraction pattern extends to about 1.4 $Å^{-1}$.

Table 4 shows the displacements of the iron atom and of N_ϵ of the proximal histidine (F8) from the mean plane of the porphyrin in various derivatives. The displacements in deoxyMb are exactly the same as in the model compound 2-MeImTPPFeII and, within error, also the same as in deoxyHb; but the displacements in met and oxyMb are larger than in any of the model compounds or in the corresponding Hb derivatives, which suggests that the tertiary structure of Mb is designed to hold the iron farther from the porphyrin plane. As would be expected from this feature, its oxygen affinity is lower than that of Hb in the R structure, but only by a factor of about three and much higher than that of Hb in the T structure. In MbO_2 the oxygen molecule occupies a single ordered position with Fe–O–O = 112°. The imidazole of His F8 and Fe–O–O are approximately coplanar and eclipse the Fe–N(Pyrrol II) bond. N_ϵ of His F8 lies 2.3 Å from the mean porphyrin plane compared to 2.07 Å in the picket fence complex. One explanation for this difference and for the displacement of the iron

Table 4 Heme stereochemistry in erthrocruorin, myoglobin, and hemoglobin

Compound	Derivative	Fe–Ct[a]	Fe–porph[b]	Fe–$N_{pyrrole}$	Fe–ligand	Fe–N_ϵ	N_ϵ–porph	Angle of imidazole plane: With N_1–Fe–N_3	Angle of imidazole plane: With heme normal	Ref.
Erythrocruorin	H_2O-met	0.16	0.08	2.02	3.0	2.25	2.3	7°	0°	43
	CN-met	0.13	0.06	2.01	2.2	2.1	2.1	7°	0°	43
	CO	0.11	0.01	2.01	2.4	2.1	2.2	7°	0°	43
	O_2	0.38	0.30	2.04	1.8	2.1	2.3	7°	0°	42, 43
	deoxy	0.23	0.17	2.02	3.1	2.2	2.3	7°	0°	43
Myoglobin	H_2O-met	—	0.40	2.04	2.0 (constrained)	2.1	2.5	19°	4°	38
	CO	—	0	—	—	—	2.3	19°	—	40
	O_2	0.16	0.26	2.05	2.0	2.1	2.3	6°	4°	41
	deoxy	—	0.55	2.06	—	2.1	2.6	19°	11°	39
Hemoglobin	H_2O-met α	—	0.07	2.0 (constrained)	2.0 (constrained)	2.1	2.2	21°	—	59
	H_2O-met β	—	0.21	2.0 (constrained)	2.0 (constrained)	2.2	2.4	15°	—	59
	CO α	—	0.04	—	—	—	—	—	—	61
	CO β	—	0.2	—	—	—	—	—	—	61
	deoxy α	—	0.60	2.1	—	2.0	2.6	20°	8°	10
	deoxy β	—	0.63	2.1	—	2.2	2.8	25°	7°	10

[a] Ct, center of porphyrin N's.
[b] porph, mean plane of porphyrin N's and C's, including the first C's of each side chain.

atom toward the proximal side in MbO_2 may be sought in the orientation of the imidazole with respect to the porphyrin. In MbO_2 this imidazole eclipses the Fe–N(pyrrole II & IV) bonds, while in the picket fence complex the imidazole plane lies at about 45° to them, which minimizes van der Waals repulsion and maximizes overlap of the Fe *d* orbitals with the π orbitals of the imidazole nitrogen. In MbO_2 repulsion is maximized and overlap minimized. The oxygen molecule is also constrained to the eclipsed orientation by steric hindrance of the distal residues Phe CD1, Val E11, and His E7.

In metMb the sixth coordination position at the iron atom is filled by a water molecule which lies at a distance of about 2 Å from the iron and is hydrogen-bonded to N_ϵ of the distal E7 His at a distance of 2.8 Å; it is also in van der Waals contact (3.2 Å) with methyl γ_2 of Val E11. In deoxyMb the sixth coordination position is empty, and the distal His side chain swings inwards and away from the position where the heme-linked water molecule has been. A positive peak lies at a distance of 3.2 Å from its N_ϵ, farther inside the heme pocket than the heme-linked water in metHb and at a distance of 3.0 Å from one of the pyrrolic carbons; this may be a weakly bound water molecule. In MbCO the heme is planar and the CO oxygen is displaced 0.8 Å from the heme axis into the heme pocket (40); the distal His is within van der Waals distance of the CO, but is not hydrogen-bonded to it. Similar bending was found in horse HbCO (45). This is surprising because the Fe–C–O line in iron carbonyls is normally straight; the bending in MbCO and HbCO was found to be due to steric hindrance by methyl γ_2 of Val E11, and N_ϵ of His E7. Bending of the CN group in cyanmetMb (46) and in lamprey and horse cyanmetHb probably arises from the same cause (47, 48).

The azide ion in metMb (49) and metHb (50) is also inclined to the heme axis, but more steeply than CN or CO (111° between N–N–N and the porphyrin plane) in a form characteristic for covalently linked azide (4). Clearly, steric hindrance by the distal residues in the heme pocket does not permit the azide ion to lie on the heme axis, as it might in an ionic complex.

SURROUNDINGS AND STRUCTURE OF THE HEME IN ERYTHROCRUORIN Erythrocruorin (CTIII) is a monomeric Hb from the larva of the fly Chironomus tummi with a tertiary structure similar to that of myoglobin, but rather different coordination of the heme (43, 51, 52). The porphyrin is inverted, so that pyrroles 1 and 2 with their asymmetrically placed methyls and vinyls are interchanged and the convex side points toward the distal ligands rather than toward the proximal His as in myoglobin. (For numbering of pyrroles see Figure 3.) The β carbon of the vinyl on pyrrole 1 occupies a fixed position, but that at pyrrole 2 does not appear

on the electron density map, which shows that it must be rotating freely about the pyrrole–Cα bond. Fermi (10) had found a similar situation in human deoxyHb. The distal Val E11 found in vertebrate Hb's and Mb's is replaced by Ile; the distal His E7 does not lie in the heme pocket, but is external in all except the cyanomet derivative and forms a salt bridge with the heme propionate of pyrrole 4. The other heme propionate forms a salt bridge with Arg FG2. In Mb the propionates form salt bridges with Arg CD3 and His FG2 instead. In Mb residue F4 is Leu, E14 Ala, E15 Leu, and G8 Ile; in erythrocruorin all these positions are taken up by Phe's.

DeoxyMb has a distal water molecule hydrogen bonded to His E7 but not coordinated to the iron; deoxyerythrocruorin has a water molecule coordinated to the iron at a distance of 3.1; the iron is displaced by only 0.23 Å from the plane of the porphyrin nitrogens, compared to 0.42 Å in myoglobin and in 2-MeImTPPFeII. The displacement from the mean porphyrin plane is 0.17 Å less than that from the nitrogens, due to the reversed doming of the ring just described. While in metHb and metMb the heme-linked water molecule lies at a distance of 2.1 Å from the iron atom, this distance is 3.0 in meterythrocruorin, the same as in the deoxy-derivative, the only difference being that in the met derivative this position is fully occupied, while in the deoxy derivative it is only half occupied. At first sight this suggested that the deoxy-crystals were half oxidized to met, but careful checks excluded such an artefact. The iron atom in the deoxy derivative is only 0.06 Å farther from the plane of the porphyrin nitrogens than in the met derivative, compared to 0.15 Å in Mb, presumably because the iron is six-coordinated in deoxyerythrocruorin, but five-coordinated in deoxyMb. In the CO derivative the CO axis is inclined to the heme normal by 19° and the angle between Fe–C and the heme normal is 8°. Comparison with MbCO and HbCO is not possible because their carbon positions have not yet been determined. The deviation from the heme normal is due to steric hindrance by Ile E11. The strangest geometry is that found in oxyerythrocruorin. According to unrefined coordinates the iron atom is 0.11 Å *farther* displaced from the porphyrin nitrogens than in the deoxy derivative. The iron oxygen complex is almost linear, with an Fe–O–O angle of 170° (±20°), compared to 112° in Mb and 129° and 133° in the picket fence complex. A water molecule is hydrogen-bonded to the second oxygen atom. The cyanide complex is nonlinear with Fe–C–N = 164° and an angle of 5° between Fe–C and the heme normal. The cyanide anion pulls the imidazole of the distal His E7 into the heme pocket so that equal fractions of its electron density are found in the internal and external positions. The differences in heme stereochemistry between erythrocruorin and Mb are undoubtedly real and not due to errors in chemistry or in crystallographic analysis. They illustrate the profound influence that lattice forces can have

on the structure of the heme complex with different ligands, but the reasons for these differences are unclear, especially the extraordinary orientation of the oxygen molecule, which is at variance with theoretical predictions as well as with the picket fence and MbO_2 structures.

Tetrameric Hemoglobins

From coelacanth to man, the hemoglobins of bony vertebrates have the constitution $\alpha_2\beta_2$ and exhibit cooperative ligand binding. Crystals of the liganded (R) form of any one species are isomorphous, regardless of the valency of the iron and the nature of the ligand, and their structures have been found to differ only in details in and around the hemes. Crystals of the unliganded (T) form are unique. Table 5 shows the derivatives whose structures have been determined by X-ray analysis. The only ones to be refined and have their atomic coordinates determined are human deoxyHb and HbCO, and horse metHb. Table 4 shows their heme geometries. In human deoxyHb, the displacement of the iron from the mean porphyrin plane was calculated by a computer program which fitted a flat porphyrin to the observed electron density and allowed the iron atom to move. This resulted in a displacement of the iron from the porphyrin plane toward the proximal histidine of 0.6 Å in all four subunits. The displacement of N_ϵ of the proximal histidine (F8) from the porphyrin plane is 2.6 Å in the α- and 2.8 Å in the β-subunits. In human HbCO the displacements of the iron atoms are 0.04 Å in α and 0.21 Å in β, and the displacements of N_ϵ of His F8 are 2.2 Å in α and 2.4 Å in β. In horse metHb the displacements of the iron are 0.07 Å in α and 0.21 Å in β, and those of N_ϵ of His F8 are 2.2 Å in α and 2.4 Å in β, almost exactly the same as in human HbCO.

Table 5 Structure determinations of hemoglobins[a]

Species	Derivative	Resolution (Å)	Ref.
Human A	deoxy	2.5	10
	CO	2.8	45
	fluoromet + IHP	3.5	53
Human F	deoxy	2.5	54
Human S	deoxy	3.0	55, 56
Horse	deoxy	2.8	57
	CO	2.8	45
	NO	2.8	125
	fluoromet	2.8	58
	aquomet	2.0	59
	cyanomet	2.8	48
	azidomet	5.5, 2.8	49, 111
	metmangano	2.8	60

[a] (44) lists the abnormal Hb's solved up to 1976.

In view of the predominantly high-spin character of metHb, the displacements in the α-subunits seemed anomalously small at first but they are now seen to be consistent with the structure of the high spin TPPbisH_2OFe(III) described in the section on coordination of the iron atom, where it is shown that the constraints of the axial ligands confine the iron to the porphyrin plane. The structure of HbO_2 has yet to be determined, but if the heme is planar with a distance Fe–N_ϵ = 2.1 Å, as in the unhindered picket fence complex, then the proximal histidine would have to move towards the porphyrin plane by 0.6 (±0.16) Å on ligation of oxygen, coupled with transition of the entire molecule from the T to the R structure.

I have suggested that the low oxygen affinity of the T structure is due mainly to constraints of the globin that oppose that movement of the proximal histidines. Baldwin & Chothia have now compared the structures of human deoxyHb, human HbCO, and horse metHb in detail and have discovered the stereochemical nature of these constraints. The description which follows is based mainly on their paper (8).

CHANGES IN QUATERNARY STRUCTURE Transition from the T to the R structure is brought about without significant changes at the contact which holds together the components of the αβ-dimer (i.e. the $\alpha_1\beta_1$-contact and the symmetry related $\alpha_2\beta_2$-contact). Significant changes are defined as greater than the RMS error of 0.43 Å of the individual sets of coordinates. If the interfaces of the $\alpha_1\beta_1$-dimers of human deoxyHb and HbCO are superimposed, the overall movement on ligation of the $\alpha_2\beta_2$-dimer relative to the $\alpha_1\beta_1$-dimer is an anticlockwise rotation of 14.9° and a translation of 0.8 Å. The rotation axis is normal to and intersects the molecular dyad at a point between the α-subunits 12 Å from the molecular centre, and makes an angle of 18° with the molecular x axis. The translation of 0.8 Å is along the same axis as the rotation, and toward the molecular centre (Figure 5).

The hemoglobin tetramer is formed by association of the $\alpha_1\beta_1$-dimer with the $\alpha_2\beta_2$-dimer. The C helix and FG corners of α_1 contact the FG corner and C helix of β_2 in both deoxy and liganded forms. The change of quaternary structure results from a large movement of about 6 Å at the contact between α_1C and β_2FG and a small movement at the contact between α_1FG and β_2C, [see Figure 7 of (44)].

CHANGES IN TERTIARY STRUCTURE Having noted the absence of significant changes at the $\alpha_1\beta_1$-interface Baldwin & Chothia superimposed the electron density maps of human deoxy and HbCO at this interface and used it as a reference frame to search for differences in atomic coordinates due to changes in tertiary structure. They found that the following helical segments show no significant shifts: Bα and β, Cα, Dβ, Gα and β, and

Hα and β, except for the last few residues. Clear differences are seen for the hemes, the F and F' helices, (the F' helix is made up of residues usually referred to as EF5 to EF8), the FG segments of both subunits, and helix Eβ. The remaining regions show differences that are marginally significant. Figure 6 shows the important changes. On ligation the heme of the α-subunit moves 0.6 Å farther into its pocket in a direction parallel to heme nitrogens N_1 and N_3; the backbone of helix F moves 0.4 Å perpendicular to and toward the heme plane. It also moves the same distance as the heme parallel to CH_1–CH_3 and about 1 Å more than the heme parallel to CH_2–CH_4. The helix also tilts and turns relative to the heme with Ala F9

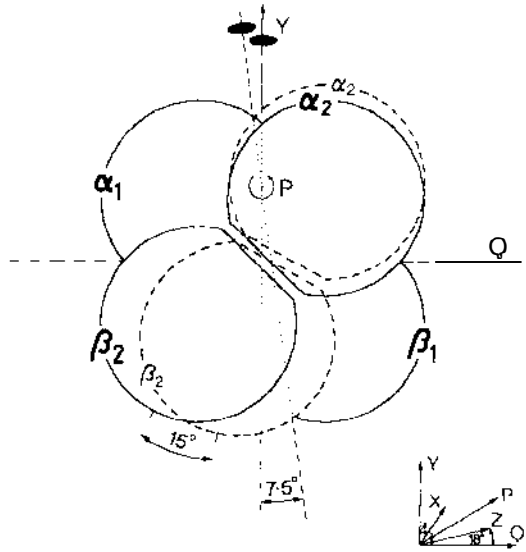

Figure 5 Schematic diagram illustrating the rotation of the $\alpha_2\beta_2$ dimer relative to $\alpha_1\beta_1$ that occurs in the quaternary structure change from deoxyHb (solid lines) to HbCO (broken lines). The molecule is viewed along the rotation axis (P) which intersects the molecular dyad of deoxyHb (Y) at the point shown. The relationship between this view and the standard molecular axes is shown in the bottom right-hand corner. Y is at right angles to X, Z, P, and Q. In addition to the rotation, the $\alpha_2\beta_2$ dimer moves into the paper by 0.8 Å.

The detailed geometry of the quaternary change is given below for the transitions from human deoxy to human HbCO and to horse metHb.

	deoxy/CO			deoxy/met		
Direction cosines of rotation axis	0.951	0.006	0.309	0.948	0.003	0.319
Rotation angle		−14.9°			−12.3°	
Shift along rotation axis		+0.8 Å			+1.19 Å	
A point on rotation axis	−0.03	11.91	−0.13	0.05	17.94	−0.32

Figures 5–9 and their captions are reproduced, with permission, from (8).

moving toward the heme plane and across toward pyrrole 3. A change of conformation at His FG1 and Lys FG2 allows the helix F and especially His F8 to tilt toward the heme without the side chains of Leu FG3 and Val FG5 altering their positions relative to the heme plane. The F' helix continues the motion of the F helix, but the turn parallel to the heme plane is lost and the motion is almost parallel to CH_2–CH_4. Helix E also turns and tilts slightly relative to the heme plane, but its center hardly moves perpendicular to that plane. Residues FG3 to G4 shift as illustrated in Figure 6, with little change in the conformation of the main chain. The side chain of Leu FG3 and Val FG5 show small changes of conformation to stay in contact with the heme. The movements of these residues are dissipated in the next two turns of helix G but Phe G5 and Leu G8 move in the same direction as the heme, toward the central cavity of the molecule. Residues H18 to HC1 adapt their main chain conformation slightly to the changes in the

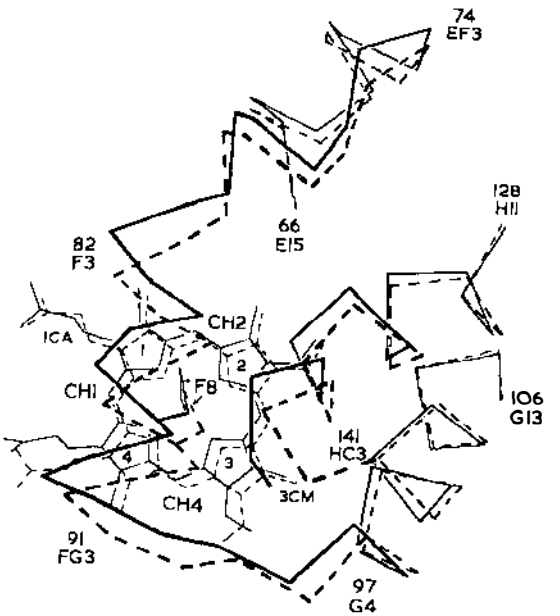

Figure 6 The tertiary structure changes that occur in the subunit on ligand binding. The figure shows Cα atoms, some of which are labeled, the hemes, and the side chain of His 87(F8) in deoxyHb (solid lines), and HbCO (broken lines). The relative positions of the two structures are derived by superimposing residues at the $\alpha_1\beta_1$ interface as described in the text. The view is perpendicular to the plane of the hemes. The 0.6 Å shift of the heme in the N1–N3 direction is clearly seen, as is the shift of the FG corner, and the F helix. The movements fade out at the beginning of the G helix and in the EF corner. 3CM denotes the methyl of pyrrole 3, 1CA the α-carbon of propionate 1.

adjacent helices, F and F'. In deoxyHb the C-terminal Arg HC3 has its α carboxyl salt bridged to Lys H10 and Val NA1 of the opposite α chain. Its side chain is salt-bridged to Asp H9 and also to an anion that lies between it and Val NA1 of the opposite α-chain. In the map of HbCO Arg HC3 has little density and must be rotating freely; the same is partly true of Tyr HC2 whose OH is hydrogen-bonded to CO of Val FG5 in deoxy, but spends only some of its time hydrogen-bonded to that group in HbCO.

The differences in tertiary structure in the β-subunits are similar to those in the α-subunits. The relative positions of the hemes and the E, F, G, and H helices of deoxyHb and HbCO are shown in Figure 7. On ligation the heme moves 1.5 Å farther into its pocket parallel to N_1–N_3 and rotates by 9.6° about an axis joining N_2 to N_4. This moves pyrrole 1 toward the side chain of Lys E10 and pyrrole 3 toward the side chain of Phe G5. The shifts of helices F and F' are similar to, but slightly smaller than, those in the α-subunit. The side chains of Phe F1, Leu F4, and His F8 move slightly

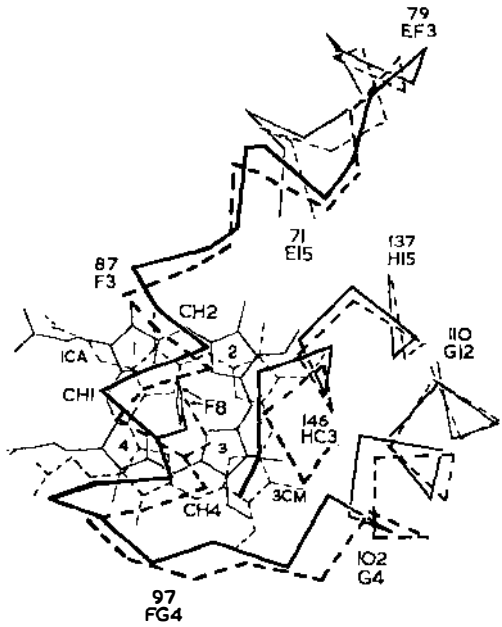

Figure 7 The tertiary structure changes that occur in the β-subunit on ligand binding. The figure shows Cα atoms, the hemes, and the side chain of His 92(F8), in deoxyHb (solid lines), and HbCO (broken lines). The relative positions are derived by superimposing the residues at the $\alpha_1\beta_1$ interface as described in the text. The view is perpendicular to the plane of the heme in deoxyHb. The figure illustrates the 1.5 Å shift of the heme in the N1–N3 direction but its 9° rotation about an axis close to the N2–N4 direction is not apparent in this projection. For the sake of clarity only part of the E helix is shown.

to stay in contact with the heme. Cys F9 points out into the solution in deoxy and into the pocket between helices F and H in HbCO, the pocket having been vacated by Tyr HC2. Helix E tilts and turns relative to the heme plane. In deoxyHb the heme ligand site is blocked by $CH_3(\gamma_2)$ of Val E11 which lies only 3.5 Å from the heme centre. On ligand binding, the shift and rotation of the heme combine with the small shift of helix E to increase that distance to 4.9 Å, thus removing the obstruction to ligand binding. In deoxyHb, His HC3 has its α-carboxyl salt bridges to Lys C5α and its imidazole to Asp FG1 of the same β-chain; Tyr HC2 has its OH hydrogen bonded to CO of Val FG5, as in the α-subunit. In HbCO both these residues are freely rotating.

The similar motions of helix F relative to the heme in the α- and β-subunits have important effects on the proximal histidines. In deoxyHb, the imidazole rings are in asymmetric positions with respect to the hemes (Figures 8a and 8b). The imidazole plane is approximately normal to the heme and its projection on the heme plane is a line at about 20° to the line joining the nitrogens of pyrroles 1 and 3. The imidazole is tilted in its own plane so that C_ϵ–N_1 is 3.2 Å in α and 3.5 Å in β, while C_δ–N_3 is 3.8 Å in α and 4.2 Å in β. The distance of the iron atom from the mean plane is 0.6 Å in α and β. Note the similarity to 2-MeImTPPFeII. The changes on binding ligand, namely the translation of helix F across the hemes and the tilt of the end of helix F towards the heme, bring the histidines into positions where the imidazole rings can be made symmetrical relative to the heme by a small change of conformation of the side chains, and brought closer to the heme. Consequently in HbCO C_ϵ–N_1 is 3.1 Å in α and 3.2 Å in β, and C_δ–N_3 is 3.4 Å in α and 3.2 Å in β; the displacement of the iron from the heme plane has shrunk to 0.04 Å in α and 0.2 Å in β. Baldwin & Chothia show that the position of the heme relative to helix E in the β-subunits and the tilt of the proximal histidines relative to the hemes in both subunits are features intrinsic to the T structure which cannot be changed without a transition to the quaternary R structure, because tertiary and quaternary changes are intimately coupled. The hemes and helix F cannot move much without also moving the FG segment which forms part of the $\alpha_1\beta_2$-contact. The C helix of α_2 can make stable contacts with the FG segment of β_1 at the same time as the C helix of β_2 makes stable contacts with the FG segment of α_1 only when the two FG segments are the correct distance apart for either the T or the R structure. Due to the changes in tertiary structure this distance is 2.5 Å farther for the T than for the R structure.

SIGNIFICANCE OF STRUCTURAL CHANGES FOR LIGAND BINDING

To form a strong bond with oxygen, the iron must move from its position 0.6 Å above the plane of the porphyrin in deoxyHb into the plane in

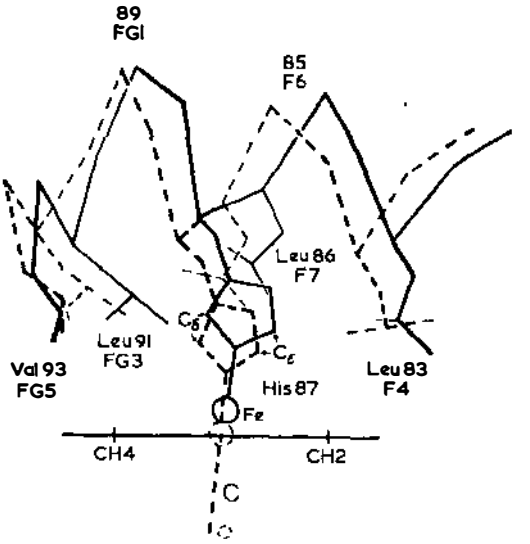

Figure 8a The positions of the F helix relative to the heme in the subunit of deoxy (solid lines) and HbCO (broken lines). The positions are shown relative to superimposed hemes. The Cα atoms of residues 81–93 are shown and also the side chains of those in contact with the heme; Leu 83, Leu 86, His 87, Leu 91 and Val 93. The heme direction CH1 – CH3 is perpendicular to the figure. The figure illustrates how, on ligand binding, the F helix moves in the CH2 – CH4 direction, and tilts toward the heme plane. The tilt is dissipated in residues 89 and 90 so that Leu 91 and Val 93 remain at the same distance from the heme plane. A figure drawn for the β subunits of deoxy and CO hemoglobins would be very similar. The angle between the plane of the imidazole and the line joining the heme center to the nitrogens of pyrroles 1 and 3 is 20°, compared to 7.4° with N_2–Fe–N_2' in 2-MeImTPPFeII in Figure 8b.

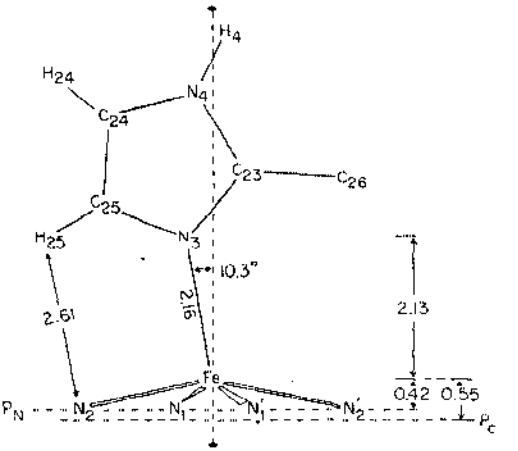

Figure 8b Structure of (2-methylimidazole)*meso*-tetraphenylporphinato FE(II) (2-MeIm-TPPFeII for short) viewed parallel to the mean plane of the porphyrin nitrogens and carbons, and nearly parallel (within 6.5°) of the imidazole plane. Fe – N_1 = 2.080 Å and Fe – N_2 = 2.091 Å. Note the similarity to deoxyHb. Reproduced by permission from (123).

HbO_2 and pull his F8 with it, which would reduce the shorter one of the two C–N distances in the α-subunits from 3.2 to 2.6 Å. However, these two atoms cannot approach closer than 3.0 Å before strong repulsion sets in. So unless the tilt can be righted, the iron atom has to stay out of the porphyrin plane, or the porphyrin N_1 must be pushed toward the distal side. In either case the iron oxygen bond would be much weakened. The spectroscopic observations described in the section on interactions between the heme and the globin indicate that in the β-subunits steric hindrance opposing the movement of the iron into the porphyrin plane is less severe, but the T structure shows the ligand position to be obstructed by $C\gamma_2$ of Val E11; this obstruction is cleared by the relative motion of the heme and helix F on transition to the R structure (Figure 9). In the α-subunit Val E11 offers no obstruction to ligand binding in either quaternary structure. The results therefore suggest that in the α-subunits the oxygen affinity of the T structure is lowered mostly by the tilt of the proximal histidine relative to the heme which opposes its movement toward the prophyrin plane, and in the β-subunits mainly by the obstruction of Val E11. This picture is consistent with the results of experiments described below.

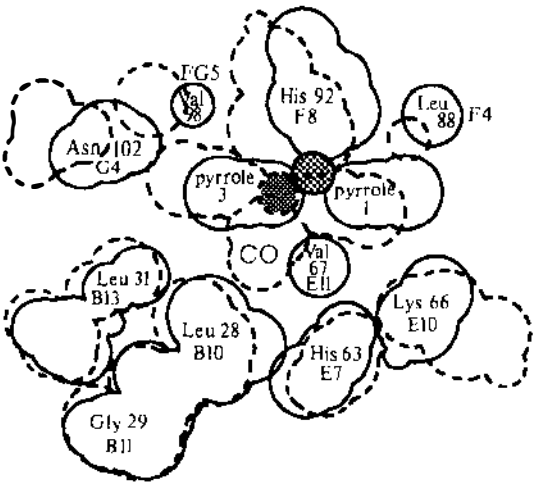

Figure 9 Space-filling diagram showing how the environment of the ligand binding site changes on going from deoxy (solid lines) to CO (broken lines) hemoglobin in the β-subunits. The figure is of a slice through a space-filling model cut so as to be perpendicular to the heme plane and to pass through N1 and N3 of the heme. In the β-subunit, room for the ligand is created by the slide (1.5 Å) and rotation (9°) of the heme. A small movement of Val 67(E11) in a direction perpendicular to the figure brings it out of the plane of the section by 0.8 Å. For the sake of clarity, the vinyl group of pyrrole 3 that occupies the space between pyrrole 3, Asn G4, and Val FG5 (see Figure 6) is omitted, as is the propionic group of pyrrole 1.

STRUCTURAL DIFFERENCES AT THE HEME IRONS BETWEEN HEMOGLOBIN AND MYOGLOBIN Table 4 compares the iron ligand geometries of the different hemoglobins, as far as they can be resolved, with those of myoglobin, erythrocruorin, and the relevant model compounds. The geometries were determined for hemoglobin by computer programs which fitted a flat porphyrin to the electron density and allowed the distance of the iron and proximal His from the porphyrin to vary so as to give the best fit. The displacement of the iron in deoxyHb is similar to that in deoxyMb, but the displacements of the iron in metHb, 0.07 Å in the α- and 0.21 Å in the β-subunits, are much smaller than the displacement of 0.40 Å in metMb, which suggests that in metHb, especially the α-subunits, repulsion between the occupied E_g orbital of the iron and the π orbitals of the porphyrin nitrogen causes an expansion of the porphyrin ring in its own plane, as in TPPbisH_2OFeIII, while in metMb the constraints of the globin favor a movement of the iron out of the porphyrin plane. Baldwin & Chothia suggest that the slightly larger displacement of the iron atom in metMb as compared to metHb may be due to the positions FG1 and FG3 being occupied by Leu and Val in the α- and β-subunits of Hb, but by the slightly longer side chains of His and Ile in Mb. This may be the explanation for the threefold lower oxygen affinity of Mb, compared to that of the R structure of Hb. This effect also causes mixed spin derivatives of Mb to have higher paramagnetic susceptibilities than the equivalent mixed spin derivatives of Hb (59): for instance at 20°C azide metMb is about 25% high-spin, while azide metHb is only about 10% high-spin.

INTERACTIONS BETWEEN THE HEME AND THE GLOBIN

For understanding heme-heme interaction the two basic questions are: how does combination of ligands with the heme irons change the quaternary structure of the globin from T to R?; and conversely, how does the change from R to T lower the ligand affinity of the heme iron? I proposed that the equilibrium between the two structures is governed by the displacement of the iron atoms and the proximal histidines from the plane of the porphyrins and by the steric effect of the ligand on the distal valines in the β-subunits (62). By the laws of action and reaction, if movement of the iron and the proximal histidine toward the porphyrin on ligand binding changes the structure from T to R, then a transition from R to T must put the gears into reverse and pull the iron and histidine away from the porphyrin. In that case the T structure should exercise a tension on the heme that restrains the iron from moving into the porphyrin plane (63). The existence of such a restraint should be detectable by physical methods. In the remainder of this review I describe experiments designed to test this hypothesis. I also de-

scribe an experiment designed to test the contribution that the obstruction by Val E11 β makes to the free energy of heme-heme interaction, even though its results were inconclusive (see the section on the role of distal residues).

Physical and Chemical Criteria for Quaternary Structure

In order to study the influence of the quaternary structure of the globin on the state of the heme, we needed a method of changing that structure without changing the sixth ligand at the heme. There are two ways of doing this: one is to use a valency hybrid in which the hemes in either the α- or the β-subunits are ferric; combination of the ferrous hemes with ligand is used to change the quaternary structure and the effect on the ferric hemes is studied spectroscopically. Alternatively, addition of the allosteric effector inositolhexaphosphate (IHP) may switch the quaternary structure from R to T. In certain fish hemoglobins the transition may be accomplished by merely lowering the pH.

The safest criterion for assessing the quaternary structure is X-ray analysis, but neither valency hybrids nor some of the complexes with IHP can be crystallized. Investigators have therefore tried to find spectroscopic and chemical criteria. These have been tested in derivatives whose quaternary structure had been determined crystallographically and then applied to those that could not be crystallized. We define the two alternative quaternary structures by the distances between the iron atoms and the structure of the $\alpha_1\beta_2$ contacts. In the R structure, $Fe(\alpha_1\text{–}\alpha_2) = 36$ Å, $Fe(\beta_1\text{–}\beta_2) = 33$ Å, Thr C3α_1 occupies the notch at Val FG5β_2 and Asp G1α_1 makes a hydrogen bond with Asn G4β_2. In the T structure, $Fe(\alpha_1\text{–}\alpha_2) = 35$ Å, $Fe(\beta_1\text{–}\beta_2) = 40$ Å, Thr C6α_1 fills the notch at Val FG5β_2, and Tyr C7α_1 makes a hydrogen bond with AspG1β_2 [see Figure 7 of (44)]. The physical and chemical criteria used to distinguish the two quaternary structures are the following.

1. *NMR* The two alternative hydrogen bonds just described give rise to two alternative exchangeable proton resonances, one at –5.8 ppm from water characteristic for the R structure and another at –10.0 ppm from water characteristic for the T structure (64).

2. *UV circular dichroism* DeoxyHb and fluoromet Hb + IHP, which have been proved to have the T structure by X-ray analysis, exhibit a prominent band of negative ellipticity with a single maximum at 287 nm. Derivatives known to have the R structure show weak positive ellipticity in this region with two slight dips near 285 and 290 nm. The negative band is due mainly to Trp C3β which lies at the $\alpha_1\beta_2$ contact (65, 66).

3. *UV spectra* Known transitions from the R to the T structure produce a UV difference spectrum (T – R) with peaks in the aromatic region at 279, 287, 294, and 302 nm. The difference in optical density between the

minimum at 283 and the maximum at 287 nm should be $\epsilon_m \geqslant 0.035$ (Figure 10). The peaks at 294 and 302 nm are due to Trp C3β (65, 66).

4. *SH reactivity* The rates of reaction of Cys F9 with *p*-mercuribenzoate or 2,2'-dithiobis(pyridine) are slowed down by the R → T transition, due to the formation of a salt bridge between His HC3β and Asp FG1β in the T structure which screens the SH group from these reagents (66). However, this effect is harder to interpret than the others because the reaction rates vary with changes of both tertiary and quaternary structure which have antagonistic effects. In the R structure the SH reactivity rises with rising spin of the β hemes, so that HbCO and Hb^+CN^- have the lowest and Hb^+F^- has the highest reactivity. This happens because low spin loosens the hydrogen bond between Tyr HC2β and Val FG5β, so that the tyrosine swings out of its pocket between helices H and F, and the SH group takes its place. High spin tightens that hydrogen bond so that the SH group is

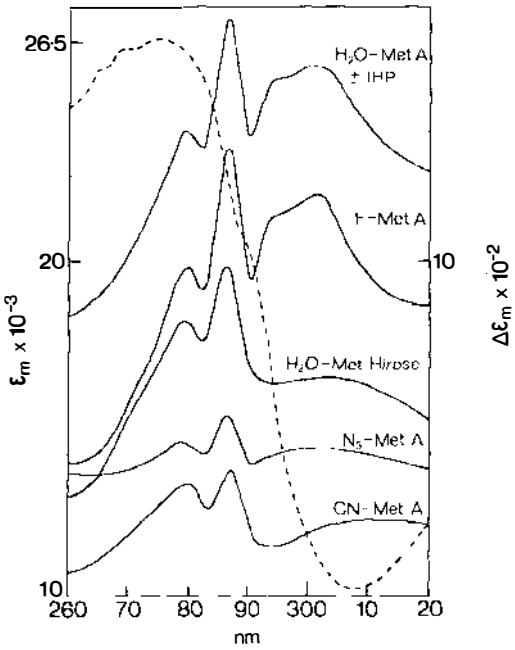

Figure 10 The broken line shows the ultraviolet absorption spectrum of human aquometHb; the solid lines show difference spectra, magnified ten times, of various human metHb derivatives ± IHP. Aquo- and fluorometHb A, and aquometHb Hirose all undergo the R → T transition, but Hb Hirose has Ser replacing Tyr at position C3β and therefore lacks the peaks 294 and 302 nm. Azide and cyanide metHb remain in the R structure which is modified by IHP in an as yet unknown manner. Reproduced by permission from (66).

excluded from the pocket and has to take up an external position instead (45, 59). In deoxyHb (T structure) the SH group is also external, but its reactivity is restricted by the surrounding salt bridge [see Figure 5 of (44)].

Methods of Changing Liganded Hb Derivatives to the T Structure

The allosteric equilibrium of valency hybrids of human Hb is governed by the spin state of the ferric irons, high spin biassing the equilibrium toward the T, low spin toward the R structure. Addition of IHP to solutions of human Hb below pH 7.0 can switch the predominantly high-spin ferric F^-, H_2O, OCN^-, SCN^-, $SeCN^-$, NO_2^-, $HCOO^-$, and CH_3COO^- derivatives to the T structure, but not the predominantly low-spin HbO_2, HbCO, Hb^+CN^-, and $Hb^+N_3^-$ (66, 67). One exception to that rule is HbNO which is low-spin, but can be switched to the T structure, because the unpaired NO electron is transferred to the d_{z^2} orbital of the iron where it weakens the $Fe–N_\epsilon$ bond (see below). There has been a suggestion that IHP can also switch HbO_2 to the T structure (68), but HbO_2 + IHP shows the exchangeable proton resonance at −6.4 ppm from water, and not the one at −9.4 ppm, which proves that it has the R structure (69).

Fish hemoglobins which exhibit the Root effect (very low oxygen affinity at pH <6.0) are more easily switched from R to T than mammalian ones. All derivatives, no matter whether high- or low-spin, can be switched to the T structure by lowering the pH and adding IHP, but the pH at which the transition occurs is lower the lower the spin state of the complex; in structural terms this implies that the number and energy of the salt bridges needed to stabilize the T structure is greater the lower the spin of the heme irons (Figure 11).

The validity of the criteria used by my co-workers and myself for the T structure has been questioned because aquometHb + IHP does not show the same SH reactivities and tetramer-dimer dissociation constants as deoxyHb + IHP. This argument typifies a widespread misunderstanding of the hemoglobin system for which I must perhaps blame myself, because I have failed to emphasize sufficiently the distinction between changes in tertiary and quaternary structure, and the associated thermodynamic states. In solution the two quaternary structures can be distinguished by spectroscopic criteria which reflect mainly the structure of the $\alpha_1\beta_2$ contact. On the other hand *thermodynamic properties* such as ligand affinities, SH reactivities, etc, must be interpreted with caution, because they depend on the *equilibrium* between R and T which varies with the spin state and ligation of the hemes and with the many other reciprocal interactions between tertiary and quaternary structures and their surrounding ions.

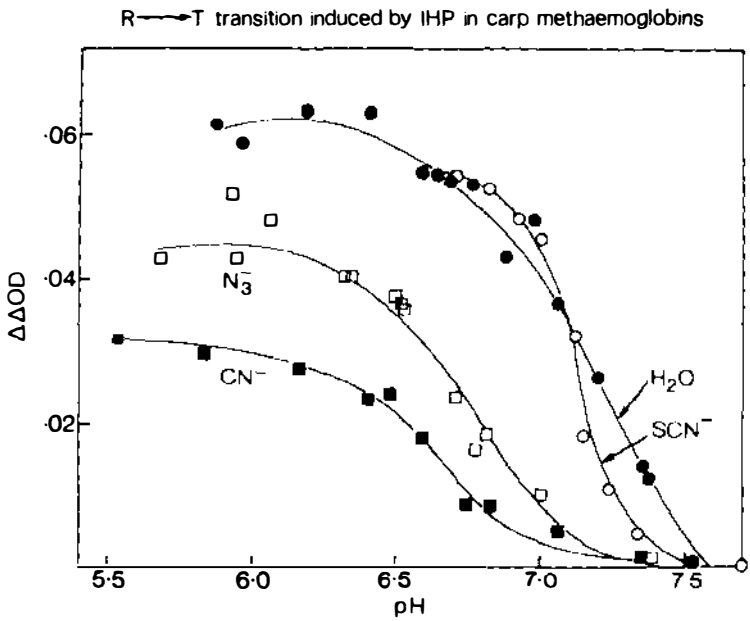

Figure 11 Magnitude of IHP-induced absorbance change between 293 and 287 nm plotted against pH for carp thiocyanide (○) metHb, aquo (●), azide (□), and cyano (■). Note the influence of the spin state of the heme on both the magnitude of the spectral change and the pH at which the R → T transition sets in. Reproduced by permission from (67).

Effects of Changes in Quaternary Structure on the Heme

In this section I consider the effect of changes in quaternary structure on the spectral and magnetic properties of the heme in a variety of derivatives of human and fish hemoglobins. Some of the changes cannot yet be interpreted; those that can, show that the predicted restraint exists in certain six-coordinated derivatives in the T structure. Its energy equivalent can be gauged from changes in thermal spin equilibria of mixed spin derivatives.

DEOXYHEMOGLOBIN Gibson (70) first observed a change in the Soret (γ) band on transition from what are now known to have been deoxyHb dimers to tetramers in the T structure; fuller descriptions of the spectral changes have been given by Brunori et al (71) and by Perutz et al (65). They consist of blue shifts of the Soret, visible, and near infrared bands, together with the appearance of a shoulder at 590 nm flanking the peaks at 556 nm. The spectral changes in mammalian and fish Hb's are similar. Sugita (72) showed that they are due almost entirely to the hemes in the α-subunits. I tentatively interpreted them in terms of increased $Fe–N_\epsilon$ distances in the

T structure, but so far there is no support for my interpretation from other experiments, nor has any alternative interpretation been proposed.

The hyperfine shifted heme proton resonances of deoxyHb differ in the R and T structures. In the T structure they lie at −7.4, −12, and −17.5 ppm from HDO; in the R structure at −7.6, −11.4 and −15.3 ppm from HDO. The first two resonances are due to the α-, and the third to the β-subunits. Note that in the NMR spectrum the main change appears in β-hemes (73). The origin of these resonances and the reasons for their shifts are unknown. Significant changes between deoxyHb in the R and T structures have been observed in the resonance Raman spectra which are sensitive to changes in conformation of the porphyrin (121, 124) but not in X-ray absorption fine structure which is sensitive to changes in Fe–N bond length (77), or in the magnetic susceptibility (65).

LIGANDED FERROUS HEMOGLOBINS Absorption spectra of mammalian HbO_2 and HbCO in the T structure have been observed only in the abnormal human Hb Kansas (Asn G4(102)β→Thr) (78). In fish Hb's showing the Root effect, the absorption spectra of HbCO in the T structure are observable, but not those of HbO_2, because the oxygen dissociates. As far as can be judged, the spectral changes in mammalian and fish Hb's are the same. In HbCO the Soret band is red-shifted by about 1 nm on transition from R to T; the difference spectrum is the exact reverse of that seen in deoxyHb. The visible α- and β-bands show slight red shifts and the β-band develops a shoulder at 580 nm (79–81). The visible changes in HbO_2 are similar but the red shifts are larger, and the shoulder appears at 583 nm (78).

HbNO proved the most revealing of the ferrous derivatives. The R → T transition gives rise to blue shifts and reduction in intensity of the α-, β-, and γ-bands, and the appearance of high-spin bands at 495, 518, and 603 nm, even though the complex remains low-spin [$S = 1/2$, Figure 12, (78, 82)]. Studies of hybrid Hb's show that these spectral changes are due mainly to the α-subunits, just as in deoxyHb. HbNO in the R structure shows a single infrared stretching frequency characteristic for six-coordinated nitrosyl hemes; transition to the T structure causes the appearance of a second infrared band, of intensity equal to the first, characteristic of five-coordinated hemes (83). Similarly, HbNO in the R structure shows an ESR spectrum similar to that of six-coordinated nitrosyl hemes, while HbNO in the T structure shows a composite of five- and six-coordinated nitrosyl hemes (84). Similar results have been obtained from comparisons of the resonance Raman spectra of five- and six-coordinated nitrosyl hemes with those of HbNO in the R and T structures (85, 86). Taken together, these results imply that in the R structure all four hemes are six-coordinated, but

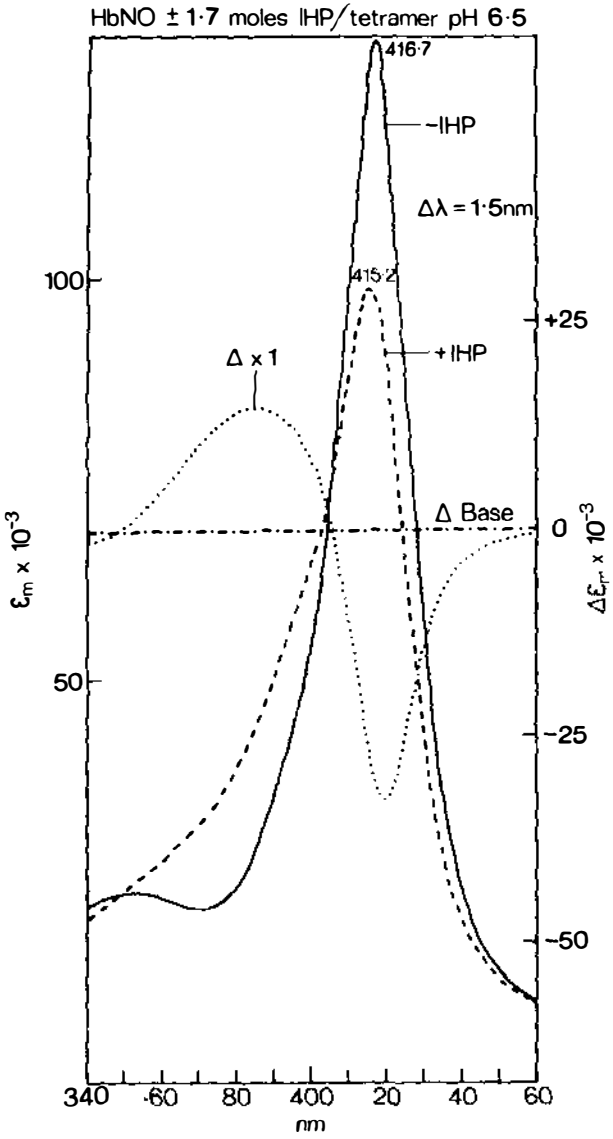

Figure 12 The Soret band of human HbNO ± IHP and difference spectrum. Most of the spectral change is due to the rupture of the Fe–N_ε bond in the α-subunits. Reproduced by permission from (78).

in the T structure only the hemes in the β-subunits remain six-coordinated; those in the α-subunits become five-coordinated, the iron histidine bond having been broken by the restraints that impede the movement of the proximal histidine toward the porphyrin. This experiment corroborates the restraint at the α-hemes in the T structure due to the tilt of the proximal histidines deduced by X-ray analysis, but it does not determine its energy equivalent, though kinetic experiments showed that an activation energy of 17 kcal/mol was needed to break the Fe–N_ϵ bond (78, 87, 88). The bond breaks because occupation of the antibonding Fe d_{z^2} orbital by the unpaired NO electron has weakened it.

LIGANDED FERRIC HEMOGLOBINS FluorometHb is pure high-spin ($\mu_e = 5.9$ BM; $S = 5/2$) and aquometHb, at 20°C, a mixed-spin derivative ($\mu_e = 5.3$ BM) above the transition temperature, which obeys the Curie law and contains high- and low-spin components in proportion to their spin degeneracies (89). The same may be true of cyanate metHb. In aquometHb in the R structure a water molecule is coordinated to the iron at a distance of 2.1 Å and hydrogen-bonded to the distal histidine at a distance of 2.8 Å (59). In fluorometHb in the R structure the fluoride ion takes up the same position as the heme-linked water in aquomet, but the fluoride ion is hydrogen-bonded to both the distal histidine and, for part of the time, to another water molecule deeper inside the heme pocket (58).

In these derivatives the R → T transition shifts all heme absorption bands to the red or produces shoulders on their red edge, just as it does in the ferrous, low-spin HbO_2 and HbCO (90). There is a decrease in OD at the positions of the low-spin bands even though there is no change in magnetic susceptibility. I tentatively interpreted the red shifts of the near infrared charge transfer bands in terms of lengthened Fe–N bonds, but so far there is no firm evidence to support this. A difference Fourier synthesis of fluorometHb in the T structure minus deoxyHb A showed a large positive peak on the distal and a negative peak on the proximal side of the α-heme, as though the iron atom had moved from its position 0.6 Å on the proximal side of the porphyrin either into the porphyrin plane or beyond it to the distal side, but the resolution of 3.5 Å was insufficient to solve the structure (53). Asher et al (91) have tentatively identified resonance Raman peaks at 443 and 471 cm^{-1} as Fe–F stretching frequencies and found that these remain unchanged on addition of IHP. If their assignment is correct then the Fe–F constellation must be the same in the two structures.

The water proton relaxation of aquometHb shows a large paramagnetic effect which proves that the iron is accessible to water protons approaching it to within 3.4 Å. These protons exchange with the bulk water at a rate

of 10^4 s^{-1} and with an activation energy of only 7.4 kcal mol^{-1}, which suggests that proton rather than water transfer is involved. Addition of IHP causes these water protons to dissociate three times more rapidly from their sites near the iron atoms, presumably because the water molecules are bound more loosely in the T than in the R structure. In fluorometHb proton exchange is much faster than in aquometHb. In this case the results allow the distance of the proton from the iron atom to be calculated as 4.11 Å in the R and 3.94 Å in the T structure (92). Anderson did an X-ray analysis of human metHb in the T structure, but unfortunately the resolution of 3.5 Å does not allow its Fe – H_2O distances to be compared with those of metHb in the R structure, so that we are not yet able to interpret those interesting magnetic effects (116).

CyanometHb is a pure low-spin compound [$\mu_e = 2.23$ BM, (93); $\mu_e = 2.59$ BM, (89)]. CyanometHb's of fish which show the Root effect can be switched to the T structure, but this has no significant effect on either the optical (67) or the resonance Raman spectra (76), presumably because all six iron ligand bonds are so strong that the steric strains of the T structure are dissipated elsewhere.

We now come to the class of ferric derivatives which have provided the most useful information concerning the effect of changes of quaternary structure on the state of the heme. These are the mixed-spin derivatives in which there exists a thermal equilibrium between the spin states of $S = 5/2$ and $S = 1/2$. The derivatives investigated include hydroxyl, azide, thiocyanate, and nitrite metHb (67, 89). The spectral changes induced by the R → T transition in these derivatives include blue shifts of the Soret band, increases in intensity of the visible high-spin bands and of the charge transfer bands in the near infrared, and decreases in intensity of the low-spin bands (Figure 13). The most striking spectral changes were seen in nitrite metHb of carp which has the red color characteristic of low spin ferric Hb's in the R structure and the brown color characteristic of high spin ferric Hb's in the T structure. The significance of this color change is discussed in the section on high pressure and magnetic measurements.

Magnetic measurements of human hemoglobins by NMR indicated that the R → T transition caused the paramagnetic susceptibility of hydroxymetHb to rise by 45% and that of thiocyanatemetHb by 11%. Human azide metHb cannot be converted to the T structure, but two abnormal Hb's form valency hybrids which allowed the effect of the R → T transition on the paramagnetic susceptibility of the α- and β-subunits to be measured separately by infrared absorption spectroscopy. This showed that in the R structure the α-hemes are less than 10% high spin, while in the T structure with IHP the high-spin fraction rises to 27%. The high-spin fraction of the β hemes in the R structure is probably about 10%; in the T structure with

IHP it rises to 35%. In trout IV and carp azide metHb measurements of the magnetic susceptibility and of the azide-stretching frequencies showed a rise of the high-spin fraction in the tetramer from about 10% in the R structure to 50% on the T structure, which is equivalent to a free energy change of ~ 1 kcal per mol heme. All these measurements were done at a

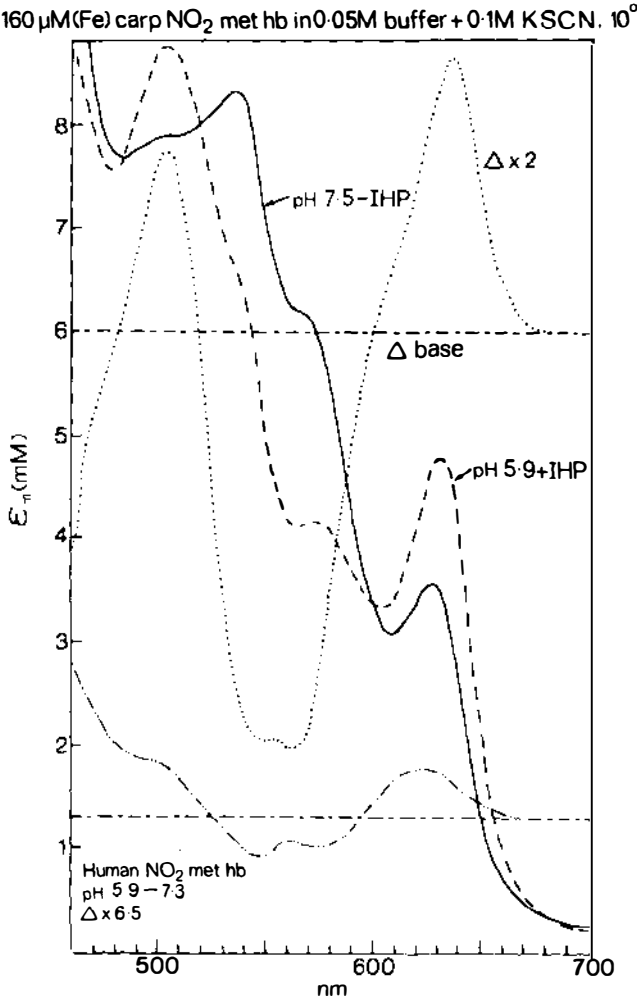

Figure 13 Visible spectra of carp NO_2metHb [– IHP at pH 7.5 (R structure), and + IHP at pH 5.9 (T structure)] and difference spectrum magnified two times. The —·—·— curve shows the pH-dependent difference spectrum of human NO_2 metHb which undergoes no change in quaternary structure, magnified 6.5 times. Reproduced by permission from (67).

single temperature near 20°C. Qualitatively these results showed that in mixed-spin derivatives the R → T transition causes a change to higher spin (67). We have seen, in the sections on coordination of the iron atom and the interaction between structure and spin state in iron chelates that this is equivalent to a stretching of the Fe–N bonds.

EFFECT OF QUATERNARY STRUCTURE ON THERMAL SPIN EQUILIBRIA (89) Most ferric iron complexes remain in the same spin state over a wide temperature range and thus obey the Curie-Weiss Law, $\chi = 1/(T-\Theta)$, where χ is the magnetic susceptibility, T is the absolute temperature, and Θ is a constant; but in some complexes the separation in energy between the low ($^2T_2$) and high ($^6A_1$) spin states is so small that it approaches the thermal energy (Figure 14). Such compounds exhibit a temperature-dependent spin equilibrium. If the low-spin state is the ground state, they show a region at low temperature where they are pure low spin ($S = 1/2$) and obey the Curie-Weiss Law; then a transitional region where their paramagnetic susceptibility rises with rising temperature until the high- ($S = 5/2$) and low-spin states are equally populated; and, finally, a region of mixed-spin where the Curie-Weiss Law is obeyed again (Figure 14). This state of mixed-spin may be contrasted with the true intermediate-spin of $S = 3/2$ which has been observed in only few synthetic compounds. One example is [Fe (III) octaethylporphin] (ClO_4) in which the coordination about the iron is square planar because the ClO_4^- is bound to the iron only very weakly (94). The state of $S = 3/2$ is best distinguished from a spin equilibrium by its temperature-dependent magnetic susceptibility and Mössbauer spectrum.

Thermal spin equilibria in metHb derivatives have been studied extensively (for review see 95), but measurements have been confined to derivatives in the R structure. Messana et al (89) have determined the effect of the R → T transition on spin equilibria by measuring magnetic susceptibilities between 300° and 90°K with a high resolution superconducting magnetometer. The derivatives used were carp azide, nitrite, and thiocyanate metHb. The authors expected to find a dependence upon $1/T$ like the theoretical curves for mixed-spin derivatives shown in Figure 14, i.e. a low-spin ground state followed by a gradual transition to higher-spin above some critical temperature, but the actual results were rather different.

At the lowest temperatures all the plots of χ versus $1/T$ were linear, (Figure 15). From the linear parts of the curves the effective magnetic moments, μ_e, could be derived:

$$\mu_e = \sqrt{\frac{3\chi kT}{N\beta^2}} = 2.828 \sqrt{\chi T}, \qquad 1.$$

where N is Avogadro's number and β the Bohr magneton. The magnetic moments are listed in Table 6. For all but one of the hemoglobins in the R structure the moments have values characteristic of low-spin heme complexes, but for all hemoglobins in the T structure and for the thiocyanate derivative in the R structure their values are intermediate between low- and

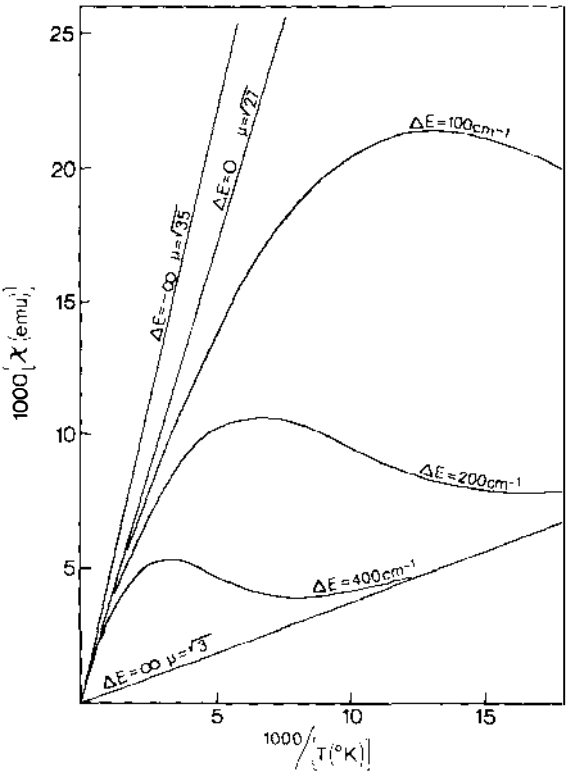

Figure 14 Temperature-dependence of paramagnetic susceptibility calculated from

$$\left(35 \exp \frac{-\Delta E}{kT} + 3\right) \Big/ \left(3 \exp \frac{-\Delta E}{kT} + 1\right)$$

where k is the Boltzman constant, T the temperature in °K, and ΔE the difference in energy between the high-spin $^6A_1$ and the low-spin $^2T_2$ states. The effective magnetic moment $\mu_e = 2.828 \sqrt{\chi_A T}$ BM. The top line, $\Delta E = -\infty$ represents a pure high-spin compound; the next, $\Delta E = 0$, a mixed-spin compound, and the lowest line, $\Delta E = +\infty$ a pure low-spin compound. The curves represent thermal spin equilibria for various values of ΔE. Note that at high temperature these all converge on to the line of $\Delta E = 0$. The low-spin case represents $\mu_e = 2\sqrt{S(S+1)} = \sqrt{3}$ BM. Due to spin orbit coupling values of $\mu_e \leqslant \sqrt{5}$ BM are known to occur. (BM = Bohr magnetons).

Figures 14–17 are reproduced, with permission, from (89).

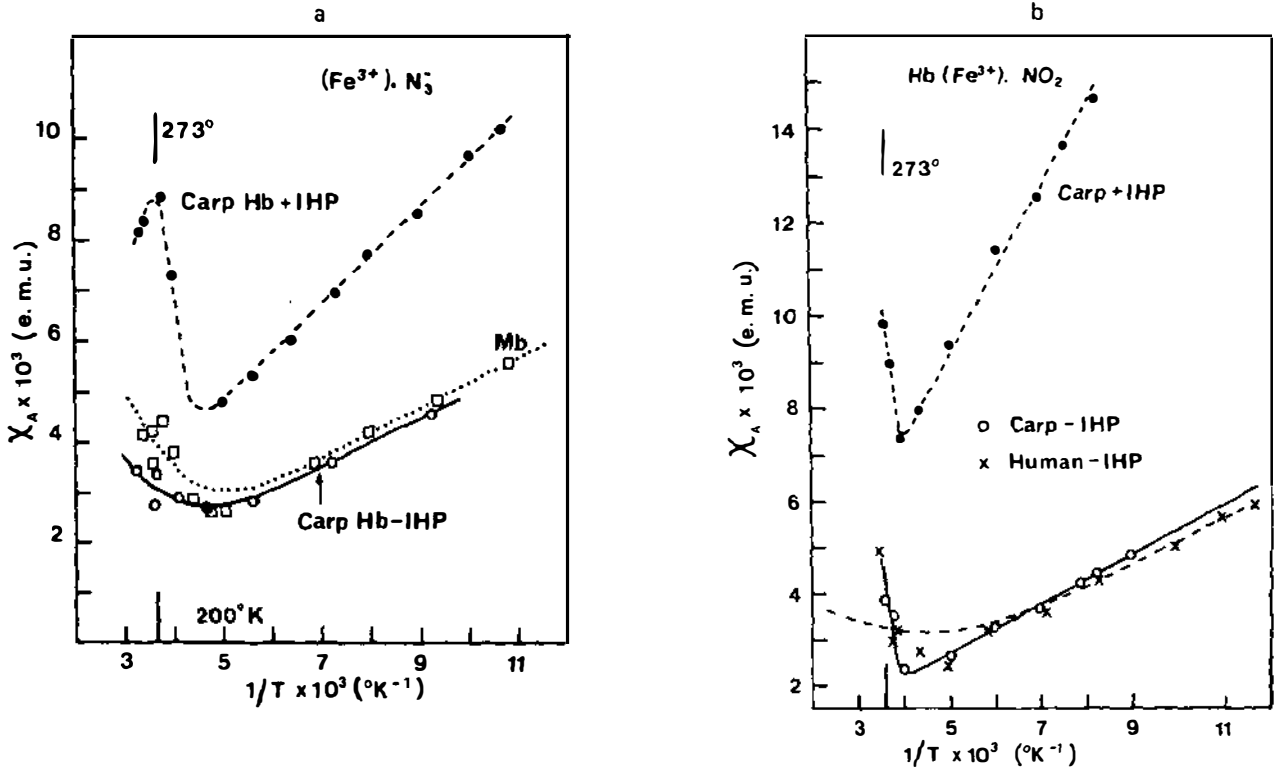

Figure 15 Magnetic susceptibilities of (*a*) azide and (*b*) nitrite metHb of carp ± IHP and of azide metMb. The dotted curve in *a* represents an attempt to fit the myoglobin data to a curve calculated from Equation 3, with the exponential term multiplied by a factor $\gamma = 10$ and with $\Delta E = 1000$ cm^{-1}. The broken line curve in *b* represents an attempt to fit the data to a curve calculated from Equation 3 with $\gamma = 1$. Note that the fit of both theoretical curves is poor.

Table 6 Effective magnetic moments of hemoglobin and myoglobin derivatives in the Curie range at low temperature

Derivative	Species	IHP	μ_e (BM)[a] (± 0.05 BM)	α[b] (high-spin fraction)
$Hb^+ NO_2^-$	carp	+	3.80	0.34
$Hb^+ NO_2^-$	carp	−	2.07	0
$Hb^+ N_3^-$	carp	+	2.80	0.12
$Hb^+ N_3^-$	carp	−	1.98	0
$Hb^+ SCN^-$	carp	+	3.49	0.26
$Hb^+ SCN^-$	carp	−	3.09	0.18
$Hb^+ CN^-$	human	−	2.59[c] (2.23)[d]	0
$Hb^+ H_2O$	human (0–30° C)	−	5.3 (± 0.1 BM)	0.78
$Mb^+ N_3^-$	sperm whale		2.03 (2.17)[d]	0

[a] BM = Bohr magnetons

[b] α is calculated by assuming $\mu^2_{LS} = 4.0$ and $\mu^2_{HS} = 35$ BM^2; $\alpha = \mu_e^2 - 4/31$

[c] The higher value of μ_e for human $Hb^+ CN^-$ than for the derivatives of carp hemoglobin – IHP must be attributed to a larger orbital contribution, since all these derivatives are low spin, $S = 1/2$.

[d] The values in brackets are those found by Iizuka & Kotani (93).

high-spin. In all instances the effective magnetic moment for the frozen hemoglobins in the T structure is larger than in the R structure. In solution, several derivatives show reverse Curie behavior characteristic of compounds in which there exists a thermal equilibrium between two spin states. This behavior persists after freezing down to temperatures of between 250 and 200°K. The magnetic moments in solution in the T structure are also larger than in the R structure (Table 7); the rise just above the freezing point varies from 1.26-fold in thiocyanate to 1.84-fold in the nitrite derivative. The 1.52-fold rise in carp azide metHb at room temperature corresponds to a 2.4-fold rise in magnetic susceptibility which agrees with the 2.5-fold increase found in the closely related trout IV azide metHb by NMR and also with the increase calculated from the change in the relative intensities of the high- and low-spin infrared azide stretching frequencies of carp azide metHb mentioned in the preceding section (67).

If a transition metal compound exhibits two alternative spin states in thermal equilibrium, their populations should be proportional to

$$W_L \exp -\frac{E_L}{kT} \text{ and } W_H \exp -\frac{E_H}{kT} \qquad 2.$$

where W_L and W_H are proportional to the spin degeneracies $(2S_L + 1)$ and $(2S_H + 1)$, and E_L and E_H are the energies of the low- and high-spin states. If $\Delta E = E_H - E_L$, and μ_L and μ_H are the magnetic moments of the low-

Table 7 Rise in effective magnetic moment μ_e of carp metHbs on addition of IHP in solution

		−IHP		+IHP	
Derivative	T	μ_e	α[a]	μ_e	α
N_3^-	275°	2.6	0.09	4.4	0.50
	300°	2.9	0.14	4.4	0.50
SCN^-	275°	3.9	0.36	4.9	0.64
NO_2	275°	2.5	0.07	4.6	0.56

[a] α is the fraction high spin, calculated as in Table 5.

and high-spin states respectively, the paramagnetic susceptibility χ_{Fe} should follow the equation

$$\chi_{Fe} = \frac{1}{8T} \frac{\frac{2S_H + 1}{2S_L + 1} \exp -\frac{\Delta E}{kT} \quad \mu_H^2 + \mu_L^2}{\frac{2S_H + 1}{2S_L + 1} \exp -\frac{\Delta E}{kT} + 1}; \qquad 3.$$

$$\chi_{Fe} = \frac{1}{8T} \frac{K\mu_H^2 + \mu_L^2}{K + 1}, \text{ where } K = \frac{[HS]}{[LS]} \qquad 4.$$

i.e. the equilibrium constant between the high- and low-spin states.

However, Iizuka & Kotani (93, 96) found that this was not true of any of their metMb or metHb derivatives; the initial fall of χ with $1/T$ was always steeper than predicted by the simple theory. The results of Messana et al (89) confirmed their findings.

Iizuka & Kotani (93, 96) were able to fit their data by allowing the equilibrium constant K in Equation 4 to have the more general form

$$K = \exp(-\Delta G/RT) = \exp\left(-\frac{\Delta H - T\Delta S}{RT}\right), \qquad 5.$$

with constant, empirically chosen values for ΔH and ΔS.

A difficulty in applying the procedure of Iizuka & Kotani to fit the data of Messana et al by means of Equations 3–5 was that the empirical values of μ_L^2 (as determined from the slope of the χ versus $1/T$ plots at low temperature and listed in Table 6) for the T state Hb's were much higher than the maximum plausible value of about 6 BM^2 expected for the low spin $S = ½$ state.

A plausible hypothesis to account for this anomaly is to suppose that below some temperature, T_0, the globin and surrounding ice become too

rigid to accommodate the change in iron bond lengths that accompany spin changes, so that a random mixture of high- and low-spin hemes becomes frozen in and thermal equilibrium cannot be attained at temperatures below T_0; this hypothesis may be incorporated into Equation 5 by assuming that for temperatures below T_0 the equilibrium constant K has the fixed value $K = K(T_0)$. Such freezing-in of spin equilibria has been observed by Mössbauer spectroscopy in cyanate metMb (97) and in [Fe (II) 2-aminomethylpyridine)$_3$]$^{2+}$I$_2$ (98).

Messana et al determined the parameters of Equations 4 and 5 required to fit their data for the azide derivatives by means of a least squares procedure in which the values $\mu_H^2 = 35$ BM^2 and $\mu_L^2 = 4.0$ BM^2 were assumed. The data for azide metHb – IHP were fitted together with a single pair of values, ΔH, ΔS; in fitting the data for azide Hb + IHP the additional parameter T_0 was included to represent the temperature below which the spin equilibrium is assumed to be frozen-in. A reasonably good fit between theory and experiment was obtained when Equation 4 was plotted for the values $\Delta H = 2.6$ kcal mol^{-1} and $\Delta S = 5.7$ cal mol^{-1} deg^{-1} for Hb–IHP; and with $\Delta H = 2.4$ kcal mol^{-1}, $\Delta S = 8.3$ cal mol^{-1} deg^{-1}, and freeze-in temperature $T_0 = 193$°K for Hb + IHP. However, the values of ΔH and ΔS were subject to considerable uncertainty, especially in the case of Hb + IHP, because the two parameters are highly correlated ($C = -0.99$) in the fitting procedure. This situation can be illustrated graphically by replotting the data in terms of the apparent equilibrium constant K', between the high and low spin states, defined as

$$K' = \frac{8\chi T - \mu_L^2}{\mu_H^2 - 8\chi T} \qquad 6.$$

The right-hand side of Equation 6 is the solution of Equation 4 for K; hence, if the data fit Equations 4 and 5, then $K' = K$ and

$$-\ln K' = \frac{\Delta G}{RT} = \frac{\Delta H}{R}\frac{1}{T} - \frac{\Delta S}{R},$$

so that ΔH and ΔS can be determined from the slope and intercept, respectively, of a plot of $-\ln K'$ against $1/T$. Such a plot is illustrated in Figure 16; the straight lines are drawn to correspond to the values of ΔH and ΔS corresponding to the curves in Figure 15.

The equilibrium at temperatures below $T_0 \approx 200$°K appears to be frozen-in, so that K' is constant below that temperature. Thus, it is only the data in the narrow range $1/T = 3\text{–}5 \times 10^{-3}$ deg^{-1} that can be used to determine the values of ΔH and ΔS, and these data are too meager to determine separately the slope and intercept of the fitting lines. However, if it is

accepted that a simple spin equilibrium does obtain within this temperature range, then one can estimate the free energy difference $\Delta(\Delta G) = \Delta G$(-IHP) $- \Delta G$(+IHP) that stabilizes the high spin state in Hb + IHP relative to its stability in Hb – IHP. Since the vertical scale in Figure 16 is $\Delta G/RT$, the separation in height of the data points ± IHP gives $\Delta(\Delta G/RT)$. Thus at 300°K the difference in –lnK' is about 1.5–2.0; therefore $\Delta(\Delta G) = (1.5–2.0) \times 1.98$ cal mol^{-1} deg$^{-1} \times 300$ deg $= 0.9–1.2$ kcal, in agreement with the value

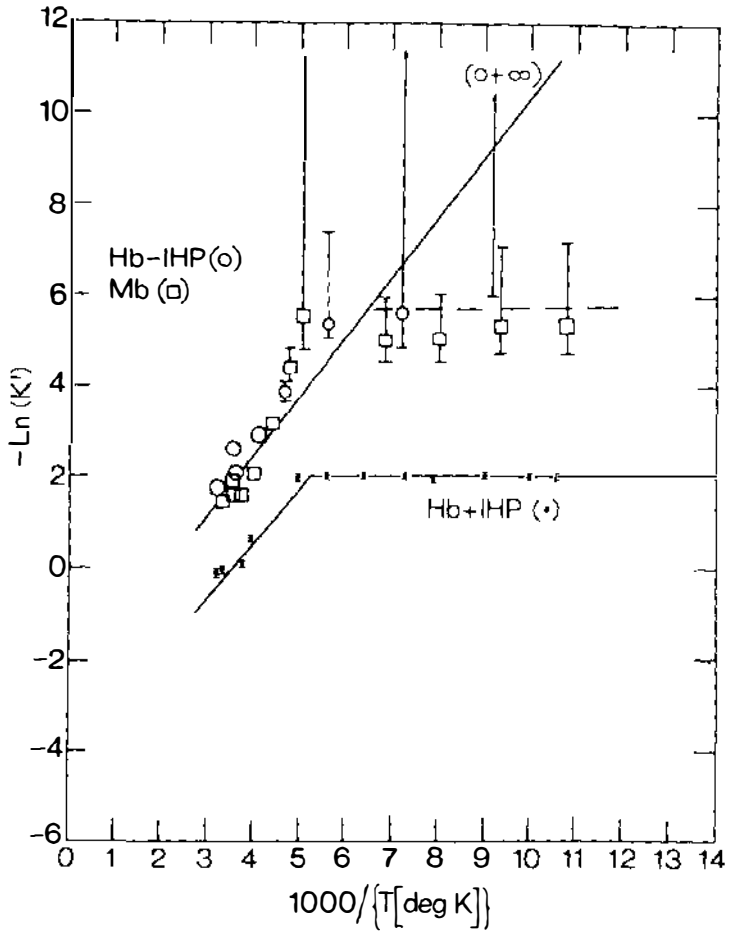

Figure 16 Data of Figure 15*a* and theoretical curve of spin equilibria in R and T structures plotted as the negative logarithm of the apparent equilibrium constant, K', calculated from Equation 4 with $\mu_H^2 = 35$ BM^2 and $\mu_L^2 = 4.0$ BM^2. Error bars are drawn for an arbitrarily assumed error of ±3% in χ; they become very large when the compound approaches pure low spin and K' tends to infinity. (BM = Bohr magnetons.)

derived from the infrared measurements mentioned in the preceding section. At 250°K the difference is 1.3–2.3, so that $\Delta(\Delta G) = 0.6$–1.1 kcal.

A survey of the literature on the magnetic properties of synthetic iron chelates shows that there is nothing unique about the properties of Hb. If the rise in χ with T in the non-Curie portions of the Hb curves is steeper than predicted from Boltzmann statistics with weighting based on spin degeneracy alone, this is also true of the majority of synthetic iron chelates. The only compound I could find that does follow Boltzmann statistics based on such weighting is crystalline $[FE(II)(5R\text{-phenanthroline})_2(SCN)_2]H_2O$, where R is either Cl or NO_2 (98). Most magnetic work has been done on crystalline powders which often show very sharp transitions from low to high-spin at some critical temperature, probably because of cooperative effects in the crystal lattices; but even iron complexes in solutions show steeper transitions than predicted by the simple theory (21, 99–101). In crystalline samples, plots of the spin equilibrium constant against $1/T$ are often nonlinear, showing that there is not a simple intramolecular equilibrium; in solution such plots are mostly linear. If the spin equilibrium constant is defined as in Equation 4 and the low-spin state is the ground state, then ΔH and ΔS are always positive, but ΔS is always larger than the value of 2.2 kcal/mol expected from the change in spin degeneracy alone. The excess ΔS has been attributed to the stereochemical changes accompanying the spin changes.

Finally, one might envisage that an intermediate-spin state of $S = 3/2$ might play a part in some of the phenomena observed here, but this has been found only in porphyrins where axial bonds are either absent or extremely weak, such as the [FE (III) octaethylporphin] (ClO_4) structure already mentioned (94). It is unlikely, therefore, that this spin state exists in any of the Hb compounds, but the question can be answered with certainty only by Mössbauer spectroscopy. A pure $S = 3/2$ state is ruled out for azide metHb of carp in the T structure because its squared magnetic moment is far below 15 BM^2.

PRESSURE-DEPENDENCE OF PARAMAGNETIC SUSCEPTIBILITY IN MIXED-SPIN DERIVATIVES A change to higher spin is expected to involve a lengthening of the Fe–N distances (see Tables 1 and 2) and should therefore be accompanied by an expansion in molecular volume. Conversely, a volume contraction produced by hydrostatic pressure should bring about a transition to lower spin. The pressure dependence of the spin equilibrium should allow determination of the volume change accompanying the spin transition.

The pressure-dependence of the visible absorption spectra of Hb and Mb derivatives has been studied extensively (102–105). High-spin metHb in

which the sixth ligand is weakly bound are reversibly denatured, at pressures as low as 1 kbar at some pH's, to a low-spin form in which the distal imidazole probably becomes the sixth ligand. Low-spin derivatives such as cyanomethemoglobin, in which the iron ligand bonds are much stronger, can withstand pressures of up to 8 kbar without denaturation. There have also been studies of the effect of pressure on the electronic and Mössbauer spectra of ferric iron porphyrins that showed the appearance of mixed- or intermediate-spin states and a reduction of the iron to the ferrous state (106). However, the pressures used in these experiments ranged from 20–140 kbars, whereas those in the experiments reviewed here did not exceed 4 kbars.

Messana et al (89) used a pressure bomb that recorded optical rather than magnetic changes, and concentrated on the azide derivatives, because the relationship between their optical absorption and paramagnetic susceptibilities can be calibrated on the basis of both magnetic measurements and infrared spectra. Assuming values of $\chi = 0.014$ and 0.0022 emu for the high- and low-spin components respectively, the authors showed that the absorption coefficient ϵ_m (630 nm) is related to α, the fraction of high-spin component, by the equation $\alpha = 0.032 + 0.348(\epsilon_{630}-2)$. Absorption at the high-spin band, at 630 nm, was found to rise, and at the low-spin bands, at 541 and 573 nm, to fall with rising pressure. These spectral changes were reversible and took place at lower pressures than the gross spectral changes that characterize denaturation. From the spectral changes the spin equilibrium $K = [^6A_1]/[^2T_2]$ was calculated as a function of pressure (Figure 17). Thermodynamics gives

$$[\partial (\ln K/\partial P)]_T = -\Delta V/RT \qquad 7.$$

where ΔV is the change in volume that occurs when protein containing one mole of heme is converted from the high- to the low-spin form. The volume changes derived from Equation 7 and Figure 17 are as follows:

	$-\Delta V$ (ml/mole heme)
Sperm whale azide metMb	12.5 ± 1.7
Carp azide metHb – IHP	6.7 ± 1.3
Carp azide metHb + IHP	13.3 ± 1.0

This shows that the transition from the high- to low-spin state is accompanied by a volume contraction, as in other iron chelates, and that in Hb in the T structure this contraction is twice as large as in the R structure. The contraction in Mb is near to that in the T structure of Hb.

DISCUSSION OF HIGH PRESSURE AND MAGNETIC MEASUREMENTS

The volume changes associated with $^6A_1 \rightarrow {}^2T_2$ transition in azide metMb and Hb are in the same direction as those observed in simple iron chelates,

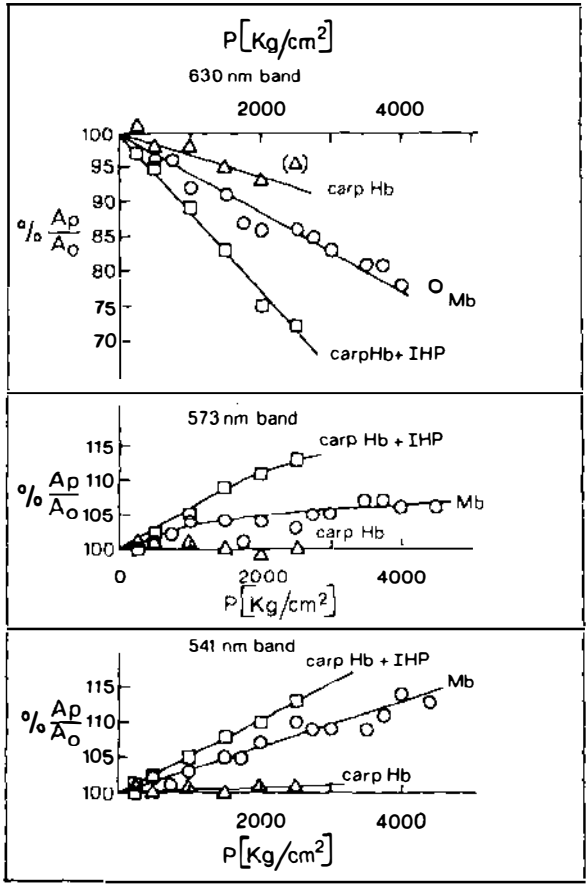

Figure 17a **Effect of hydrostatic pressure *P* on the optical densities of the visible absorption bands of Mb and carp Hb ± IHP. A_P = optical density at pressure *P*; A_o = optical density at atomospheric pressure. All bands have been corrected for compression of water.**

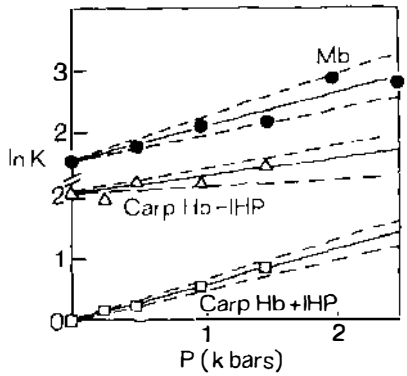

Figure 17b **Spin equilibria (*K*) calculated from Figure 17a (top) as a function of hydrostatic pressure (*P*). The broken lines indicate the error limits.**

but larger. For instance, the volume changes associated with the spin transitions of the octahedral FeS_6 complex in [Fe (III) tris(dithiocarbamate)] were between 3.7 and 4.1 ml/mol, depending on the value assumed for $\mu_e(^2T_2)$. A molecular model showed that the solvent would have relatively free access to the FeS_6 core, and the authors therefore felt justified in assuming the entire volume change to be due to a change in radius of that core. Taking Fe–S = 2.75 Å, this gave a contraction in Fe–S bond length of 0.07 Å (99). In azide metHb, the maximum likely contraction in average Fe–N bond length would be from 2.10 to 1.98 Å. If the solvent had access to the Fe–N core, this would produce a volume change of 3.7 ml/mol, close to the value found in the irondithiocarbamate. In fact, the volume changes observed in azide metHb are 6.7 ml/mol in the R and 13.3 ml/mol in the T structure. This means that there must be stereochemical changes in the protein associated with the spin transition and these must be larger in the T than in the R structure, presumably because the changes in Fe–N distances themselves are larger.

In going from 300° to 200–250°K the magnetic moments of all Hb derivatives drop much more steeply than can be accounted for by the difference in spin degeneracy of the $^2T_2$ and $^6A_1$ states. Again, this must be due to stereochemical changes in the surrounding protein. We do not know what these are, but the simplest proposition would be that they consist mainly in changes in the width of the heme pocket. A rough calculation shows that thermal contraction of the heme pocket over this temperature range may be of the same order as the movement of the iron atom relative to the porphyrin plane, and could therefore magnify the influence of temperature on the *spin equilibrium*. On the other hand, the freezing-in of the spin equilibrium at 250°–200°K implies that *spin transitions* cannot take place without structural changes in the protein which require a thermal activation energy greater than $\Delta E(^2T_2–^6A_1)$.

The large spectral and susceptibility changes observed in nitrite and thiocyanatemetHb may be connected with the fact that each of these ligands can combine with transition metals in two alternative ways—M–ONO or M–NO_2; M–SCN or M–NCS. In the first mode of ligation they lie nearer the high-spin and in the second nearer the low-spin end of the spectrochemical series. The first example of an M–ONO $\rightleftharpoons$ M–NO_2 isomerization was discovered by Jorgensen in $[Co(NH_3)_5NO_2]$ Cl_2 in 1894; it is sterically possible because NO_2 is not linear: the angle O–N–O = 134°. There is no reason why such isomerization should not take place in these Hb derivatives on transition from the R to the T structure; inversion of the ligand on transition from low to high-spin would weaken the Fe–ligand bond so that the steric requirements of the T structure could be satisfied by stretching it.

IMPLICATIONS FOR HEME-HEME INTERACTION All the measurements on carp and trout azide metHb point to the same answer, namely that in the T structure ΔE, the free energy gap between the six-coordinated high- and low-spin states is about 1 kcal/mol heme lower than in the R structure. This answers the question as to the energy equivalent of the restraint that opposes transition to the low spin state in the T structure, when the only chemical difference between the heme complexes in the two alternative quaternary structures consists of a change of spin. It amounts to about one third of the energy equivalent of the difference in oxygen affinity between the R and T structures of carp Hb. However, in the reaction with oxygen the change in spin is accompanied by a change in coordination number, so that the contribution made by the spin change cannot be separated experimentally from that due to the steric effects of the oxygen. Furthermore, the change of spin occurs in the ferrous form where the difference in energy between the high and low spin states is larger. Finally, it is important to realize that the ligand affinities of the α- and β-subunits in fish Hb's exhibiting the Root effect are very unequal. The free energies of heme-heme interaction of the two different subunits reacting with CO in menhaden Hb are 3.6 and 1.95 kcal/mol heme; it is not yet clear to which subunits these should be assigned (89). This heterogeneity suggests that the large changes in magnetic susceptibility are concentrated mainly in one pair of subunits, so that their free energy equivalent per heme would amount to 2 kcal/mol, compared to either 1.95 or 3.6 kcal/mol for the free energy of heme-heme interaction of either one or the other pair of subunits. The free energy of heme-heme interaction of the reaction with CO is generally equal to that with oxygen.

So much for the physical measurements to determine the energy equivalent of the restraint that opposes transition to the low-spin state in the T structure. Collman and his collaborators (107, 108) asked whether restraint of the kind I had envisaged could actually lead to a reduced oxygen affinity. They measured the thermodynamic constants of oxygen binding to some of the cobalt and iron picket-fence complexes, described in the section on coordination of the iron atom, with either N-methylimidazole or 1,2-methylimidazole as the fifth ligand. The former combines with the cobalt or iron atom without steric hindrance, while the latter is restrained by close contact of the 2-methyl group with the porphyrin, so that it opposes the movement of the metal atom into the plane of the porphyrin on ligation with oxygen, in the same way as I imagined the globin does in the T structure of Hb. The results show that the mean oxygen affinity (p_{50}) for the unhindered N-methyl cobalt complex is 150 torr, compared to 960 torr in the hindered 1,2-methylimidazole cobalt complex. In the iron complexes the corresponding values are 0.59 and 38 torr, corresponding to a difference in

free energy of oxygen binding of 2.5 kcal/mol, comparable to the free energy of heme-heme interaction in Hb. The answer to the question asked at the beginning of this paragraph is therefore in the affirmative, restraint does lead to reduced oxygen affinity.

On the basis of this, or indeed of any theory of heme-heme interaction, one would have expected the Fe–O bond to be weaker in the T than in the R structure, weaker bonds being normally associated with lower affinity. Nagai et al (121) have tested this point by Resonance Raman Scattering, but found the Fe–O stretching frequency of HbO_2 to be within $5cm^{-1}$ the same in the two structures. Their result seems paradoxical, but they have proved it beyond any reasonable doubt. They point out that a frequency shift of 28 cm^{-1} should have been observed if the free energy of heme-heme interaction of 3 kcal/mol were stored in the iron oxygen bond, or a shift of 40 cm^{-1}, if the bond had been stretched by 0.02 Å in the T structure, as suggested by Warshel (110). Nagai et al have not measured the Fe–N_ϵ stretching frequency in HbO_2, and it remains to be seen if this bond is stretched in the T structure. More probably, their result implies that in HbO_2 in the T structure nearly all the free energy is stored in the protein rather than the heme, because the protein is "softer" and could take up strain energy in hydrogen bonds, van der Waals interactions, and a variety of small torsions. By contrast, in the mixed spin derivatives discussed above, the heme itself is "soft," in the sense that the spin equilibrium is readily shifted to the high-spin state with the longer Fe–N bonds.

THEORETICAL STUDIES OF HEME-HEME INTERACTION

Investigators have also tried to find out if my mechanism is reasonable on theoretical grounds. Gelin & Karplus (109) used empirical energy functions and structural data to calculate the most likely change in conformation of the heme complex on ligation and the pathway of its transmission to the subunit boundaries. They discovered the tilt of the proximal histidines, described in the section on changes in tertiary structure, as the source of the restraint to oxygenation in the T structure. They suggested that movement of the proximal histidines towards the porphyrin would force a change of tilt of the hemes which in its turn would trigger stereochemical changes at the subunit boundaries.

Warshel (110) used a different approach. He calculated the distribution of potential energy of the heme complex in Hb by molecular orbital theory, taking care to calibrate his potential functions from known structures and vibrational frequencies of metal porphyrins. He asked where the energy that determines the observed conformations of iron porphyrins comes from,

where the free energy of heme-heme interaction arises, and where it is stored. He found that the pyramidal structure of five-coordinated high spin hemes is due both to the high-spin iron being too large for the size of the porphyrin hole, and to the steric repulsion between fifth ligand and the porphyrin, in agreement with the structural data reviewed in the section on the coordination of the iron atom. However, the potential well that keeps the five-coordinated high-spin iron out of the porphyrin plane has gentler slopes than that of the well that confines the six-coordinated low-spin iron to the porphyrin plane, because the iron nitrogen bonds and the van der Waals interactions between the porphyrin and the distal ligands are stronger. In other words, it costs less energy to push the iron atom of deoxyHb into the porphyrin plane than to pull the iron of HbO_2 out of the plane.

Warshel calculated the energies of the deoxygenated and oxygenated T and R structures. In agreement with Gelin & Karplus, his results indicated that the largest part of the free energy of heme-heme interaction is concentrated in only one of these four forms, namely the oxygenated T structure. He calculated that its low oxygen affinity is paid for by stretching the Fe–O bond by 0.02 Å and the Fe–N_ϵ bond by 0.004 Å, and by displacing the iron atom from the porphyrin plane by 0.03 Å; but mainly it is paid for by straining the surrounding protein. However, the structure of the sterically hindered picket fence complex shows that these estimates of bond stretching are too low; in fact the Fe–O bond is stretched by 0.15 Å and the Fe–N_ϵ bond by 0.10 Å (see the section on the coordination of the iron atom). Warshel's calculated iron displacement agrees with the observed one. Difference electron density maps of ligated Hb in the T structure do indeed show strain in the protein in the T structure, concentrated mainly in helix F and the FG segment, but they show much greater strain in deoxygenated Hb in the R structure. The constancy of the Fe–O stretching frequency (121) speaks against significant stretching of the Fe–O bond.

EXTENDED X-RAY ABSORPTION FINE STRUCTURE

Eisenberger et al (77) have challenged the decisive role played by the movement of the iron atom and the proximal histidine relative to the porphyrin plane in the allosteric mechanism of Hb on the basis of their extended X-ray absorption fine structure (EXSAF) determination of the iron-nitrogen bond distances in Hb. This new method measures the absorption of X-rays at wavelengths just below the absorption edge of the iron atom. At these wavelengths absorption is modulated by interference with low-energy photoelectrons scattered by neighboring atoms. From this inter-

ference pattern the distance between the iron atom and its neighbors can be calculated (117). The method has the great advantage of being applicable to amorphous materials and has recently led to a proposal for a tentative structure of the active Fe–Mo–S complex in nitrogenase.

Eisenberger et al used it to determine the $Fe–N_{porph}$ distances in human deoxyHb and N-MeImTpivPPFe(II) compared to HbO_2 and N-MeImTpivPPFe(II)O_2. Their absorption spectra for deoxyHb and the oxygen-free picket complex are identical, as are the spectra for HbO_2 and the oxygenated picket fence complex. For the oxygenated forms they calculate $Fe–N_{porph} = 1.979(\pm 0.1)$ Å, in agreement with the X-ray crystallographic measurements. For the deoxygenated forms they find $Fe–N_{porph} = 2.055$ (± 0.003) Å, substantially shorter than in any high-spin five-coordinated iron porphyrin, either ferrous or ferric (see Table 8). The reason for this anomalous result is unclear. Eisenberger et al now argue that if the distance from the center of the porphyrin ring to the nitrogens is 2.055 Å, as observed in 2-MeImTipvPPFe(II), the strain energy needed to expand the ring so as to accommodate the iron in its own plane would be smaller than the thermal energy, and therefore the iron position is being determined only by the steric requirements of the axial ligand, now no longer counterbalanced by a sixth ligand. However, we have seen in the section on the stereochemistry of iron porphyrins and related compounds that in fact these requirements and electronic factors play a roughly equal part in displacing the iron atom from the porphyrin plane, and theory shows that the geometry of a five-coordinated transition metal complex cannot be predicted from Morse potentials, but requires molecular orbital calculations. Such calculations indicate that only low-spin d^6 complexes prefer a square pyramidal conformation with an angle $\Theta = 90°$ between apical and basal bonds (112). High-spin complexes in which the d_{z^2} orbital is occupied favor a pyramid with $\Theta > 90°$. A molecular orbital calculation carried out on a model $Fe(NH_3)_5^{2+}$ showed that the low-spin system has an energy minimum at $\Theta = 90°$. A high-spin system in which both d_{z^2} and $d_{x^2-y^2}$ are singly occupied, as in deoxyHb, had its minimum at $\Theta = 112°$, which corresponded to the iron atom being 0.77 Å out of the plane of the four nitrogens, even though there was no constraint on the center-to-nitrogen distance.

Eisenberger et al suggest that doming and buckling of the porphyrin may play a more important part in the Hb mechanism than the movement of the iron atom. In theory this could produce just as viable a mechanism, provided it leads to a movement of the proximal histidine relative to the mean porphyrin plane, but in fact there is no evidence that doming is any greater in deoxyHb than in the 2-MeImTPPFeII structure described in the section on the stereochemistry of the iron porphyrins, where the porphyrin nitrogens are out of the mean porphyrin plane by only 0.13 Å. Baldwin & Chothia (8) find that on transition from deoxy to HbCO the hemes shift and

turn relative to the globin, but they find no change in heme conformation other than the movement of the iron atom.

The strongest evidence for the pyramidal geometry of the Fe–N complex in unstrained five-coordinated high-spin iron porphyrins comes from the many known structures. Table 8 contains no instance where the iron atom is displaced from the plane of the porphyrin nitrogens by less than 0.4 Å; the mean displacement is 0.46 Å. In addition, the porphyrin nitrogens are displaced from the mean plane of the carbons toward the iron by an average of 0.043 Å. In ferric iron porphyrins the $Fe–N_{porph}$ bond distance is never less than 2.060 Å; in ferrous ones it is at least 0.01 Å longer. The geometry of 2-MeImTPPFeII corresponds closely to that of the heme in deoxyMb which is sufficiently well resolved for us to be sure of its structure. Only where the high-spin ferrous iron has acquired a weak sixth ligand does the iron atom lie closer than 0.4 Å to the plane of the porphyrin nitrogens. One such example is the polymeric picket fence complex catena-{μ-[meso-Tetrakis($\alpha,\alpha,\alpha,\alpha$-*o*-pivalamidophenyl)- porphinato-N,N',N'',N''':O]-aquo-iron(II)-tetrahydrothiophene},{Fe(TpivPP)(OH_2)(THT)} for short (122). Here a water molecule is coordinated to the iron at a distance of 2.9 Å and in consequence the distance of the iron from the plane of the porphyrin nitrogens is reduced to 0.32 Å. A similar situation is found in deoxyerythrocruorin where a water molecule is coordinated to the iron atom at a distance of 3.1 Å and the iron atom is displaced only by 0.23 Å from the plane of the porphyrin nitrogens (43).

Table 8 Parameters of five-coordinated high-spin iron porphyrin complexes from crystal structure data[a]

Compound	Fe–Ct (Å)[b]	Δ (Å)[c]	$Fe–N_{porph}$ (Å)
O [Fe III (Di MeOEP)] $_2$	0.512	0.018	2.065
O [Fe III (TPP)] $_2$	0.496	0.044	2.087
Fe III (TPP) Br	0.489	0.070	2.069
Fe III (TPP) (NCS)	0.485	0.068	2.065
Fe III (TPP) I	0.480	0.068	2.066
Fe III (Proto) Cℓ	0.474	0.080	2.062
Fe III (Meso-DME) (OCH_3)	0.456	0.034	2.073
Fe III (Proto-DME) (SR)	0.434	0.015	2.064
Fe II (TPP) (2-Me-Im)	0.418	0.134	2.086
Fe II (T piv PP) (2-Me-Im)	0.399	0.027	2.072
Fe III TPP Cℓ	0.389	0	2.060
Average	0.457	0.051	2.069

[a] I wish to thank Dr. Lynn Hoard for this table. For references to these structures see (4).

[b] Ct is at the centre of the porphyrin nitrogens.

[c] $\Delta = (Fe \ldots P_C) - (Fe - P_N)$ where P_C is the mean plane of the porphyrin carbons and P_N the mean plane of the porphyrin nitrogens.

ROLE OF DISTAL RESIDUES

The roles of the distal His E7 and Val E11 have been studied in two abnormal hemoglobins: Hb Zürich (His E7 → Arg) and Hb Sydney (Val E11 → Ala) (113). The replacement of His E7 by Arg leaves a large gap in the heme pocket, because the Arg side chain is external and forms a salt bridge with one of the heme propionates. The gap allows small molecules easy access to the heme iron and causes hemolytic inclusion body anemia on treatment of heterozygous carriers with sulfanilamides. Hb Zürich forms the normal quaternary T and R structures, but the association constant of the first oxygen to combine with it is 7.5 times larger than for Hb A. The second order rate constant for the combination of CO with the T structure of Hb Zürich is much larger for Hb A. The partition coefficient $M = (p\,O_2[HbCO]/p\,CO[HbO_2])$ for the abnormal β subunit of Hb Zürich is 500 compared to 250 for Hb A. The rate of autoxidation in vitro and the acid catalyzed reductive displacement of superoxide by azide are faster than in Hb A. The CO stretching frequency is raised from 1952 cm^{-1} in Hb A to 1958 cm^{-1} in Hb Zürich, but the O–O stretching frequency is not affected.

These properties show that the distal histidine plays a multiple role. Its C_δ and N_ϵ atoms are in contact with pyrrole 1 of the porphyrin and oppose the rotation of the heme on ligand binding which brings that pyrrole closer to Lys E10 (see the section on changes in tertiary structure). The histidine is therefore essential for maintaining the restraint responsible for the low oxygen affinity of the T structure. It also lowers the CO affinity and thus protects Hb from CO poisoning, which is vital because of the CO produced endogenously on porphyrin breakdown. The protective mechanism may be part steric and part electronic. Sterically the histidine helps to force the CO into the off axial orientation which probably weakens the Fe–C bond. The sp^2 orbital of N_ϵ overlaps the empty π^* antibonding orbital of the carbon. $sp^2 \rightarrow \pi^*$ donation would weaken the CO bond and reduce the CO stretching frequency, in accordance with observation. It would also weaken $d\pi \rightarrow \pi^*$ donation from the iron to the CO, thus weakening the Fe–C bond, but this is a second order effect. Finally, the distal His protects the iron from oxidation. It has a pK of only 5.4, so that at physiological pH its single proton must be on either N_δ or on N_ϵ. It has been argued that it is on N_ϵ and forms a hydrogen bond with the bound oxygen, but if N_ϵ were permanently protonated, the distal histidine should promote rather than inhibit oxidation of the heme iron. However, the point can be settled with certainty only by neutron diffraction.

We have seen that Val E11 β obstructs the ligand binding site in the T structure. Study of Hb Sydney should have allowed us to measure the contribution which that obstruction makes to the free energy of heme-heme

interaction, but surprisingly its oxygen affinity was found to be normal. X-ray analysis provided the explanation. The space vacated by the γ_2 carbons of the valine was occupied in Hb Sydney by a water molecule attached by a hydrogen bond to His E7. Binding of oxygen requires this bond to be broken, which costs energy; on the other hand entropy would be gained by the return of the water molecule into free solution. There is no way of estimating the relative magnitudes of these two opposing effects so that the question we asked remained unanswered. Replacement of Val E11 by Ala does not alter the partition coefficient between CO and O_2 and has a smaller effect on the CO stretching frequency than the replacement of the histidine (1952–1955 cm^{-1}). [References to the literature on Hb's Zürich and Sydney are given in (113)].

CONCLUSIONS

The main theme of this article is the regulation of the oxygen affinity of the heme by the structure of the globin. In principle, this could be accomplished by inductive effects. For instance, there exists an abnormal hemoglobin in which an alanine in the heme pocket is replaced by an aspartate (Ala E14β→Asp). This Hb has an abnormally low oxygen affinity, apparently because the negative field generated by the carboxylate group opposes the formation of the iron-linked superoxide anion (118). However, analysis of the structures of normal Hb and Mb suggest that steric rather than inductive effects are dominant. They influence both the change in Fe–N bond lengths accompanying the transition from the high-spin five-coordinated deoxy to the low-spin six-coordinated oxy form and, by steric hindrance, the actual presence of the oxygen molecule at its binding site. Therefore, the physical basis of heme-heme interaction is mechanical rather than inductive.

I have not discussed the nature of the constraints that oppose the transition to the six-coordinated low-spin state of the heme in the T structure, or the mode of action of the allosteric effectors: $[H^+]$, $[Cl^-]$, $[CO_2]$, and [2,3-diphosphoglycerate]. The constraints take the form of salt bridges between neighbouring subunits, and all the allosteric effectors act either by strengthening those salt bridges or by forming additional ones. I have also glossed over the possible mechanism by which ligand binding causes rupture of the salt bridges. These aspects have been dealt with in a recent review (44).

What remains to be done? We still do not know the exact structure of HbO_2, but can only infer it from the closely related structures of HbCO and MetHb. The low temperature techniques of X-ray analysis now available may allow this problem to be solved. More challenging is the dynamic

mechanism of the Hb molecule, which we know so far only from static pictures of the end states. For instance, the heme pocket is inaccessible to oxygen unless some door opens. Frauenfelder and his colleagues have begun to study the barriers that oppose the uptake of ligands by low-temperature kinetics (119); the continuing great advances in NMR techniques may eventually allow us to reinterpret the crystallographers' static structures of proteins in dynamic terms (120).

Literature Cited

1. Dayhoff, M. O. 1972. *Atlas of Protein Sequence and Structure,* 5:51–85 Washington, DC: Natl. Biomed. Res. Found.
2. Romero-Herrera, A. E., Lehmann, H., Joysey, K. A., Friday, A. E. 1973. *Nature* 246:389–95; and 1978. *Philos. Trans. R. Soc. London* B 283:61–163
3. Goodman, M., Moore, G. W., Matsuda, G. 1975. *Nature* 253:603–8
4. Hoard, J. L. 1975. *Porphyrins and Metalloporphyrins,* ed. K. M. Smith, pp. 317–80 Amsterdam: Elsevier
5. Collman, J. P. 1977. *Acc. Chem. Res.* 10:265–72
6. Scheidt, W. R. 1977. *Acc. Chem. Res.* 10:339–45
7. Antonini, E., Brunori, M. 1971. *Hemoglobin and Myoglobin in their Reactions with Ligands.* Amsterdam: North-Holland 436 pp.
8. Baldwin, J., Chothia, C. 1979. *J. Mol. Biol.* In press
9. Perutz, M. F. 1969. *Proc. R. Soc. London* B 173:113–40
10. Fermi, G. 1975. *J. Mol. Biol.* 97:237–56
11. Dickerson, R. E., Geis, I. 1970. *Structure and Action of Proteins.* New York: Harper & Row
12. *Handbook of Biochemistry* 1968. p. J210. Cleveland, Ohio: Chem. Rubber Co.
13. Collman, J. P., Gagne, R. R., Reed, C. A., Robinson, W. T., Rodley, G. A. 1974. *Proc. Natl. Acad. Sci. USA* 71:1326–29
14. Jameson, G. B., Molinaro, F. S., Ibers, J. A., Collman, J. P., Brauman, J. I., Rose, E., Suslick, K. S. 1978. *J. Am. Chem. Soc.* 100:6769–70
15. Jameson, G. B., Rodley, G. A., Robinson, W. T., Gagne, R. R., Reed, C. A., Collman, J. P. 1978. *Inorg. Chem.* 17:850–57
16. Scheidt, R. W., Piciulo, P. L. 1976. *J. Am. Chem. Soc.* 98:1913–19
17. Scheidt, R. W., Frisse, M. E. 1975. *J. Am. Chem. Soc.* 97:17–21
18. Kastner, M. E., Scheidt, W. R., Mashiko, T., Reed, C. A. 1978. *J. Am. Chem. Soc.* 100:6354–62
19. Butcher, R. J., Ferraro, J. R., Sinn, E. 1976. *J. Chem. Soc. D:* 910–12
20. Leipold, G. J., Coppins, P. 1973. *Inorg. Chem.* 12:2269–74
21. Hoselton, M. A., Wilson, L. J., Drago, R. S. 1975. *J. Am. Chem. Soc.* 97: 1722–29
22. Sinn, E., Sim, G., Dose, E. V., Tweedle, M. F., Wilson, L. J. 1978. *J. Am. Chem. Soc.* 100:3375–90
23. Albertson, J., Oskarsson, Å. 1977. *Acta Crystallogr.* B 33:1871–77
24. Jorgensen, L., Salem, L. 1973. *An Organic Chemist's Book of Orbitals.* New York: Academic 302 pp.
25. Pauling, L., Coryell, C. 1936. *Proc. Natl. Acad. Sci. USA* 22:210–16
26. Weiss, J. J. 1964. *Nature* 202:83–4
27. Misra, H. P., Fridovich, I. 1972. *J. Biol. Chem.* 247:6960–62
28. Demma, L. S., Salhany, J. M. 1977. *J. Biol. Chem.* 252:1226–31
29. Barlow, C. H., Maxwell, J. C., Wallace, W. J., Caughey, W. S. 1973. *Biochem. Biophys. Res. Commun.* 55:91–95
30. Hoffmann, B. M., Petering, D. H. 1970. *Proc. Natl. Acad. Sci. USA* 67:637–43
31. Chien, J. C. W., Dickinson, L. C. 1972. *Proc. Natl. Acad. Sci. USA* 69:2783–87
32. Yonetani, T., Yamamoto, H., Iizuka, T. 1974. *J. Biol. Chem.* 249:2168–73
33. Gupta, R. K., Mildvan, A. S., Yonetani, T., Srivastava, T. S. 1975. *Biochem. Biophys. Res. Commun.* 67:1005–12
34. Maxwell, J. C., Caughey, W. S. 1974. *Biochem. Biophys. Res. Commun.* 60: 1309–14
35. Cerdonio, M., Congiu-Castellano, A., Mogno, F., Pispisa, B., Romani, G. L., Vitale, S. 1977. *Proc. Natl. Acad. Sci. USA* 74:398–400
36. Cerdonio, M., Congiu-Castellano, A., Calabresi, L., Morante, S., Pispisa, B., Vitale, S. 1978. *Proc. Natl. Acad. Sci. USA* 75:4916–19
37. Kendrew, J. C., Dickerson, R. E., Strandberg, B. E., Hart, R. G., Davies,

D. R., Phillips, D. C., Shore, V. C. 1960. *Nature* 185:422–27
38. Takano, T. 1977. *J. Mol. Biol.* 110: 537–68
39. Takano, T. 1977. *J. Mol. Biol.* 110: 569–84
40. Norvell, J. C., Nunes, A. C., Schoenborn, B. P. 1975 *Science* 190:568–70
41. Phillips, S. E. V. 1978. *Nature* 273: 247–48
42. Weber, E., Steigemann, W., Alwyn-Jones, T., Huber, R. 1978. *J. Mol. Biol.* 120:327–36
43. Steigemann, W., Weber, E. 1979. *J. Mol. Biol.* 127:309–38
44. Perutz, M. F. 1976. *Br. Med. Bull.* 32:195–208
45. Heidner, E. J., Ladner, R. C., Perutz, M. F. 1976. *J. Mol. Biol.* 104:707–22
46. Bretscher, M. S. 1968. *The X-ray analysis of cyanide and carboxymethylated metmyoglobin.* PhD thesis. Univ. Cambridge, Cambridge. 106 pp.
47. Hendrickson, W. A., Love, W. E. 1971. *Nature New Biol.* 232:197–203
48. Deatherage, J. F., Loe, R. S., Moffat, K. 1976. *J. Mol. Biol.* 104:723–28
49. Perutz, M. F., Mathews, F. S. 1966. *J. Mol. Biol.* 21:199–202
50. Stryer, L., Kendrew, J. C., Watson, H. C. 1964. *J. Mol. Biol.* 8:96–104
51. Huber, R., Epp, O., Formanek, H., 1970. *J. Mol. Biol.* 52:349–54
52. Huber, R., Epp, O., Steigemann, W., Formanek, H. 1971. *Eur. J. Biochem.* 19:42–50
53. Fermi, G., Perutz, M. F. 1977. *J. Mol. Biol.* 114:421–31
54. Frier, J. A., Perutz, M. F. 1977. *J. Mol. Biol.* 112:97–112
55. Wishner, B. C., Ward, K. B., Lattman, E. E., Love, W. E. 1975. *J. Mol. Biol.* 98:179–94
56. Love, W. E., Fitzgerald, P. M. D., Hanson, J. C., Roger, W. E. Jr. 1979. In *Development of Therapeutic Reagents for Sickle Cell Anemia,* ed. E. Beuzard, J. Hercules, J. Rosa. (INSERM Symp. No. 9.) Amsterdam: Elsevier; North-Holland
57. Bolton, W., Perutz, M. F. 1970. *Nature* 228:551–52
58. Deatherage, J. F., Loe, R. S., Moffat, K. 1976. *J. Mol. Biol.* 104:723–28
59. Ladner, R. C., Heidner, E. J., Perutz, M. F. 1977. *J. Mol. Biol.* 114:385–414
60. Moffat, K., Loe, R. S., Hoffmann, B. M. 1976. *J. Mol. Biol.* 104:669–85
61. Baldwin, J. M. 1979. *J. Mol. Biol.*
62. Perutz, M. F. 1970. *Nature* 228:726–39
63. Perutz, M. F. 1972. *Nature* 237:495–99
64. Fung, L. W.-M., Ho, C. 1975. *Biochemistry* 14:2526–35
65. Perutz, M. F., Ladner, J. E., Simon, S. R., Ho, C. 1974. *Biochemistry* 13: 2163–73
66. Perutz, M. F., Fersht, A. R., Simon, S. R., Roberts, J. C. K. 1974. *Biochemistry* 13:2174–86
67. Perutz, M. F., Sanders, J. K. M., Chenery, D. H., Noble, R. W., Pennelly, R. R., Fung, L. W.-M., Ho, C., Giannini, I., Pörschke, D., Winkler, H. 1978. *Biochemistry* 17:3640–52
68. Adams, M. R., Schuster, T. M. 1974. *Biochem. Biophys. Res. Commun.* 58. 525–31
69. Huang, T.-H. 1979. In preparation
70. Gibson, Q. H. 1959. *Biochem. J.* 71:293–303
71. Brunori, M., Antonini, E., Wyman, J., Anderson, S. R. 1968. *J. Mol. Biol.* 34:357–59
72. Sugita, Y. 1975. *J. Biol. Chem.* 250: 1251–56
73. Davis, D. G., Lindstrom, T. R., Mock, N. H., Baldassare, J. J., Charache, S., Jones, R. T., Ho, C. 1971. *J. Mol. Biol.* 60:101–11
74. Deleted in proof
75. Deleted in proof
76. Scholler, D. M., Hoffmann, B. M., Schrier, D. F. 1976. *J. Am. Chem. Soc.* 98:7866–68
77. Eisenberger, P., Shulman, R. G., Brown, G. S., Ogawa, S. 1976. *Proc. Natl. Acad. Sci. USA* 73:491–95
78. Perutz, M. F., Kilmartin, J. V., Nagai, K., Szabo, A., Simon, S. R. 1976. *Biochemistry* 15:378–87
79. Knowles, F. C., McDonald, M. J., Gibson, Q. H. 1975. *Biochem. Biophys. Res. Commun.* 66:556–63
80. Giardina, B., Ascoli, F., Brunori, M. 1975. *Nature* 256:761–62
81. Saffran, W. A., Gibson, Q. H. 1979. *J. Biol. Chem.* In press
82. Cassoly, R. 1974. *C. R. Acad. Sci. Ser. D:* 278:1417–19
83. Maxwell, J. C., Caughey, W. S. 1976. *Biochemistry* 15:388–96
84. Szabo, A., Perutz, M. F. 1976. *Biochemistry* 15:4427–28
85. Szabo, A., Barron, L. D. 1975. *J. Am. Chem. Soc.* 97:660–662
86. Burke, J. M., Daly, P., Wright, P., Spiro, T. G. 1979. In press
87. Salhany, J. M., Ogawa, S., Shulman, R. G. 1974. *Proc. Natl. Acad. Sci. USA* 71:3359–62
88. Salhany, J. M., Ogawa, S., Shulman, R. G. 1975. *Biochemistry* 14:2180–90

89. Messana, C., Cerdonio, M., Shenkin, P., Noble, R. W., Fermi, G., Perutz, R. N., Perutz, M. F. 1978. *Biochemistry* 17:3652–62
90. Perutz, M. F., Heidner, E. J., Ladner, J. E., Beetlestone, J. G., Ho, C., Slade, E. F. 1974. *Biochemistry* 13:2187–2200
91. Asher, S. A., Vickery, L. E., Schuster, T. M., Sauer, K. 1977. *Biochemistry* 16:5849–56
92. Gupta, R. K., Mildvan, A. S. 1975. *J. Biol. Chem.* 250:246–53
93. Iizuka, T., Kotani, M. 1969. *Biochim. Biophys. Acta* 194:351–63
94. Dolphin, D. H., Sams, J. R., Tsin, T. B. 1977. *Inorg. Chem.* 16:711–17
95. Iizuka, T., Yonetani, T. 1970. *Adv. Biophys.* 1:157–211
96. Iizuka, T., Kotani, M. 1969. *Biochim. Biophys. Acta* 181:275–86
97. Winter, M. R. C., Johnson, C. E., Lang, G., Williams, R. J. P. 1972. *Biochim. Biophys. Acta* 263:515–34
98. Renovitch, G. A., Baker, W. A. 1967. *J. Am. Chem. Soc.* 89:6377–78
99. Ewald, A. H., Martin, R. L., Ross, I. G., White, A. H. 1964. *Proc. R. Soc. London* A 280:235–57
100. Beattie, J. K., Sunin, N., Turner, D. H., Flynn, G. W. 1973. *J. Am. Chem. Soc.* 95:2052–54
101. Tweedle, M. F., Wilson, L. J. 1976. *J. Am. Chem. Soc.* 98:4824–34
102. Fabry, T. L., Hunt, J. W. 1968. *Arch. Biochem. Biophys.* 123:428–29
103. Gibson, Q. H., Carey, F. G. 1975. *Biochem. Biophys. Res. Commun.* 67: 747–51
104. Zipp, A., Ogunmola, G. B., Newman, R. G., Kauzmann, W. 1972. *J. Am. Chem. Soc.* 94:2541–42
105. Ogunmola, G. B., Zipp, A., Chen, F., Kauzmann, W. 1977. *Proc. Natl. Acad. Sci. USA* 74:1–4
106. Grenoble, D. C., Frank, C. W., Bergeron, C. B., Drickamer, M. G. 1971. *J. Chem. Phys.* 55:1633–44
107. Collman, J. P., Brauman, J. I., Doxsee, K. M., Halbert, T. R., Hayes, S. E., Suslick, K. S. 1978. *J. Am. Chem. Soc.* 100:2761–66
108. Collman, J. P., Brauman, J. I., Doxsee, K. M., Halbert, T. R., Suslick, K. S. 1978. *Proc. Natl. Acad. Sci. USA* 75: 564–68
109. Gelin, B. R., Karplus, M. 1977. *Proc. Natl. Acad. Sci. USA* 74:801–5
110. Warshel, A. 1977. *Proc. Natl. Acad. Sci. USA* 74:1789–93
111. Deatherage, J. F., Obendorf, S. K., Moffat, K. 1979. *J. Mol. Biol.* In press
112. Elian, M., Hoffmann, R. 1975. *Inorg. Chem.* 14:1058–1076
113. Tucker, P. W., Phillips, S. E. V., Perutz, M. F., Houtchens, R., Caughey, W. S. 1978. *Proc. Natl. Acad. Sci. USA* 75: 1076–80
114. Scheidt, R. W., Reed, C. A. 1979. To be published
115. Koster, A. S. 1975. *J. Chem. Phys.* 63:3284–86
116. Anderson, L. 1973. *J. Mol. Biol.* 79: 495–506
117. Cramer, S. P., Eccles, T. K., Kutzler, F., Hodgson, K. O., Doniach, S. 1976. *J. Am. Chem. Soc.* 98:8059–69
118. Anderson, N. L., Perutz, M. F., Stamatoyannopoulos, G. 1973. *Nature New Biol.* 243:274–75
119. Alberding, N., Chan, S. S., Eisenstein, L., Frauenfelder, H., Good, D., Gunsalus, I. C., Nordlund, T. M., Perutz, M. F., Reynolds, A. H., Sorensen, L. B. 1978. *Biochemistry* 17:43–51
120. Wagner, G., De Marco, A., Wüthrich, K. 1976. *Biophys. Struct. Mech.* 2: 139–58
121. Nagai, K., Kitagawa, T., Morimoto, H. 1979. *Biochemistry.* In press
122. Jameson, G. B., Robinson, W. T., Collman, J. P., Sorrell, T. N. 1978. *Inorg. Chem.* 17:858–64
123. Buckingham, D. A., Collman, J. P., Hoard, J. L., Lang, G., Radonovich, L. J., Reed, C. A., Robinson, W. T. To be published
124. Shelnutt, J. A., Rousseau, D. L., Friedman, J. M., Simon, S. R. 1979. To be published
125. Deatherage, J. F., Moffat, K. 1979. *J. Mol. Biol.* In press